A New Control Strategy for Coordinated Control of Ground Vehicle Vertical Dynamics via Control Allocation

by

Michael Karl Binder

A thesis
presented to the University of Waterloo
in fulfillment of the
thesis requirement for the degree of
Master of Applied Science
in
Mechanical Engineering

Waterloo, Ontario, Canada, 2014

Author's Declaration

I hereby declare that I am the sole author of this thesis. This is a true copy of the thesis, including any required final revisions, as accepted by my examiners.

I understand that my thesis may be made electronically available to the public.

Abstract

The scope of this thesis concerns the basic research and development of a coordinated control system for the control of vehicle roll and pitch dynamics using suspension forces as actuators. In this thesis, the following question is explored: *How can suspension control (particularly semi-active control) be generalized to control all vertical vehicle dynamics in a coordinated way, and which would ideally be integrable with modern ESC systems?* The chosen approach to this problem will be the application of the control allocation methodology for overactuated systems, which makes use of online mathematical optimization in order to realize the desired control law. Background information on vehicle dynamics and modeling, suspension control, control allocation and optimization is presented along with a brief literature review. The coordinated suspension control system (CSC) is designed and simulated. High-level controllers and control allocators are designed and their stability properties are explored. Then, the focus is shifted towards implementation and experimentation of the coordinated control system on a real vehicle. The semi-active actuators are statistically modeled along with the deployed sensors. Both the hardware and software designs are explored. Finally, experiments are designed and results are discussed. Recommendations for future inquiry are given in the conclusion of this work.

Acknowledgements

I would like to thank my advisor Dr. Khajepour for supporting and guiding me in this rather expansive project. I would also like to thank Kevin Cochran and Jeff Gransmaa for lending their technical expertise, without which the experimental part of my thesis would have been much more daunting. Finally, I would like to thank everyone I have met and befriended in my time here at the lab and at the University of Waterloo for making my stay in Canada truly a pleasure.

Dedication

This thesis is dedicated to my family, who always support me unconditionally in my endeavours.

Table of Contents

List of Tables

List of Figures

Chapter 1

Introduction

The work presented in this thesis originated out of the "Holistic Vehicle Control" (HVC) project in development at the Mechatronic Vehicle Systems Lab at the University of Waterloo and funded by General Motors Corporation (GM). The HVC project is a form of electronic stability control (ESC), whereby vehicle slip is controlled and yaw rate tracking is achieved using torque vectoring.

The goal of the HVC system is to compute an optimal distribution of forces at the tire contact patches, which generate the desired yaw moment, longitudinal and lateral forces to attain the aforementioned objectives. Such a process is an example application of *control allocation*, as it is referred to in the literature. What makes such a system interesting is its potential for generalization, that is, its potential to form a basis for a complete, unified vehicle dynamics control system, covering all elementary degrees of freedom of the vehicle system.

One of these degrees of freedom which maintains particular importance in achieving vehicle stability is roll. It is well known that excessive roll angle, as well as great lateral acceleration precipitates the phenomenon of vehicle rollover, which accounts for a great many number of annual traffic accidents in the US and elsewhere. The oft quoted figure of 9,882 deaths due to rollover in the US in the year 2000 can be found in [8]. The danger of rollover is proportionally greater for vehicles with high centers of gravity, such as SUVs. A control system which aids in the prevention of rollover thus has great utility in regards to vehicle safefy.

Another set of dynamics to be controlled are the pitch dynamics. Unlike with roll, controlling vehicle pitch has little to do with stability, but rather has utility in improving vehicle economy. If the pitch dynamics can be controlled, then the dynamic longitudinal

load transfer can be stabilized, which normalizes the vertical loads on the tires, thus improving traction and minimizing wasted energy, particularly when accelerating or braking.

The means by which the control of these *vertical dynamics*, i.e. the roll, pitch, and pure vertical motion of a vehicle, can be handled is via the vehicle suspensions. To date, most suspension control, particularly semi-active control, is actually done in isolation from the overall dynamics of the vehicle. By this, we mean that suspension controllers are principally designed with the stabilization of the individual suspension in mind, to the exclusion of the rest of the vehicle dynamics.

In this thesis, the following question is answered: *How can suspension control (particularly semi-active control) be generalized to encompass all vertical vehicle dynamics in a coordinated way, and which would ideally be integrable with modern ESC systems?* Our approach to this problem will be the application of the control allocation methodology for overactuated systems, which like other control paradigms such as *model-predictive control*, makes use of online mathematical optimization in order to realize the desired control law.

1.1 Scope

The scope of this thesis concerns the basic research and development of a coordinated control system for the control of vehicle roll and pitch dynamics using suspension forces as actuators. The control system developed herein is a new application of techniques in control allocation. The use of control allocation is to date unprecedented in the scope of semi-active suspension control, which has largely been limited to formulations designed for a single corner of the vehicle, e.g. skyhook, groundhook, and hybrid control, among others. Using control allocation, we seek to integrate the suspension controls into a framework for multiobjective vehicle control. Furthermore, though the system under study is motivated in part by the prospect of integrating it with ESC systems, all simulation and experimentation of the control system is done without such stability systems in the loop. This is largely due to the fact that there is not currently a vehicle test platform with both controllable suspensions and torque vectoring (or differential braking) systems present in the lab.

This work is focused primarily on control design, simulation, and initial testing. Though a complete vehicle dynamics control system must necessarily also possess parameter and state estimation modules, particularly for systems to be implemented in the commercial sphere, the design of such modules will largely be excluded. For the testing of the coordinated control system, all values of interest can be measured or approximated from measurements by deployed sensors. Both the design of these modules and the task of integration with ESC systems provide worthwhile directions for further research.

In the sections on design, we will consider the cases of both active and semi-active actuators. To date, semi-active suspensions remain the most commercially viable choice for controllable suspensions, with fully active systems being featured on relatively few models. Active systems, however, remain an area of active research and development and might one day become the new standard. The focus of the experimental section will be on semi-active suspensions.

1.2 Outline

The organization of this thesis proceeds as follows. In Chapter 2, background information on vehicle dynamics and modeling, suspension control, control allocation and optimization is presented along with a brief literature review. In Chapter 3, the coordinated suspension control system is designed and simulated. High-level controllers and control allocators are designed and their stability properties are explored. In Chapter 4, the focus is shifted towards implementation and experimentation of the coordinated control system on a real vehicle. The semi-active actuators are statistically modeled along with the deployed sensors. Both the hardware and software designs are explored. Finally, experiments are designed and results are discussed. In Chapter 5, we conclude our findings and give recommendations for future inquiry.

Chapter 2

Background and Literature Review

2.1 Vehicle Dynamics and Modeling

A ground vehicle is a multi-body, nonlinear dynamic system. As such, vehicle dynamics can be very complex, oftentimes more complicated than any one vehicle model can account for. The standard approach to modeling is to employ a multi-body dynamics software package such as CarSim, Adams, or MapleSim to construct a either a wholly numerical (CarSim, Adams) or symbolic (MapleSim) model for simulation purposes. The power of these software packages lies in their ability to efficiently generate and solve the equations of motion of systems with hundreds or thousands of degrees of freedom. As the complexity of a model grows, however, it can be difficult to do analysis and control design. In actuality, a multi-body system like a ground vehicle has many degrees of freedom, and simultaneously (and perhaps unfortunately), is also undersensed. As such, it can be useful to consider instead somewhat simpler models which accurately describe the *dominant* dynamic behavior of the system. The approach taken in this thesis is not to do analysis and design on any *one* complex dynamic model, but instead to use *multiple* models, each specific to describing one or two degrees of freedom with accuracy, and to combine the insights of these different models into one unifying framework for vehicle dynamics control.

In this work, we will be concerned with controlling the so-called *vertical vehicle dynamics*, i.e. the roll, pitch, and vertical degrees of freedom. In this section, we will present the dynamic models used to capture the essence of each of these degrees of freedom, which will first be used to describe suspension control in general, and later to synthesize the integrated control system in the following chapters.

2.1.1 Two-Track Vehicle Model

The *two-track vehicle model* with roll is an extension of the bicycle model which includes the roll degree of freedom and consists of two rigid bodies: the chassis and the body. The chassis is constrained to the ground and has longitudinal, lateral, and yaw degrees of freedom. The body is constrained to roll like an inverted pendulum of length h on the chassis about the longitudinal axis, or *roll axis*. The suspensions are modeled as a rotational stiffness and damping about the roll axis. The pitch and pure vertical dynamics are therefore ignored in this formulation. In the following section we derive the equations of motion for the two-track model with roll by applying the Newton-Euler formalism. This derivation is attributed to Schofield and can be found in [18, 19].

Equations of Motion

Consider an inertial frame O and let V denote the frame of the vehicle which translates in the xy-plane with velocity $(u, v, 0)^T$ and yaws with angular velocity $\dot{\psi}$. Let B denote the body frame of the vehicle, attached to V and which rolls with angular velocity $\dot{\phi}$ relative to V. We seek to derive the angular equations of motion, that is, for the roll and yaw degrees of freedom, in the vehicle frame V.

In the inertial reference frame O, Euler's equation states that the applied moments τ on a rigid body equal the rate of change of the angular momentum L, i.e.

$$\left.\frac{dL_O}{dt}\right| = \tau_O. \tag{2.1}$$

where the subscript O denotes the coordinate frame in which the quantity is computed. This relationship can be transformed into the rotating coordinate frame V via the transport theorem

$$\left.\frac{dL_V}{dt}\right|_V + \omega_V \times L_V = \tau_V \tag{2.2}$$

where $\omega_V = [0, 0, \dot{\psi}]^T$ is the angular velocity of the vehicle frame relative to the inertial frame. Substituting the definition of the angular momentum $L_V = I^V \omega$ where I^V is the inertia tensor expressed in the vehicle frame and $\omega = [\dot{\phi}, 0, \dot{\psi}]^T$ is the angular velocity of the vehicle body, we have

$$\left.\frac{d\left(I^V \omega\right)}{dt}\right|_V + \omega_V \times I^V \omega = \tau_V. \tag{2.3}$$

For brevity, we use the notation $\mathbf{c}_\phi = \cos\phi$ and $\mathbf{s}_\phi = \sin\phi$. The inertia tensor in the vehicle frame is related to the inertia tensor in the body frame I^B by the rotation tensor

$$R_B^V(\phi) = \begin{bmatrix} 1 & 0 & 0 \\ 0 & \mathbf{c}_\phi & \mathbf{s}_\phi \\ 0 & -\mathbf{s}_\phi & \mathbf{c}_\phi \end{bmatrix} \tag{2.4}$$

via the conjugation

$$I^V = R_B^V(\phi) I^B R_B^V(\phi)^T \tag{2.5}$$

where the inertia tensor in the body frame is represented by a known diagonal matrix

$$I^B = \begin{bmatrix} I_{xx} & 0 & 0 \\ 0 & I_{yy} & 0 \\ 0 & 0 & I_{zz} \end{bmatrix}. \tag{2.6}$$

Hence, the inertia tensor in the vehicle frame has the form

$$I^V = \begin{bmatrix} I_{xx} & 0 & 0 \\ 0 & I_{yy}\mathbf{c}_\phi^2 + I_{zz}\mathbf{s}_\phi^2 & (I_{yy} - I_{zz})\,\mathbf{c}_\phi\mathbf{s}_\phi \\ 0 & (I_{yy} - I_{zz})\,\mathbf{c}_\phi\mathbf{s}_\phi & I_{zz}\mathbf{c}_\phi^2 + I_{yy}\mathbf{s}_\phi^2 \end{bmatrix}. \tag{2.7}$$

Computing the right-hand side of Euler's equation for the roll and yaw equations gives

$$\begin{aligned} I_{xx}\ddot{\phi} - \dot{\psi}^2 (I_{yy} - I_{zz})\,\mathbf{c}_\phi\mathbf{s}_\phi &= \tau_x & (2.8) \\ \left(I_{zz}\mathbf{c}_\phi^2 + I_{yy}\mathbf{s}_\phi^2\right)\ddot{\psi} + 2\dot{\psi}(I_{yy} - I_{zz})\,\mathbf{c}_\phi\mathbf{s}_\phi &= \tau_z. & (2.9) \end{aligned}$$

The applied moments on the vehicle arise from the suspension stiffness k_ϕ and damping c_ϕ, and the tire contact forces. Accounting for the applied moments on the vehicle, we have

$$\begin{aligned} \tau_x &= -c_\phi\dot{\phi} - k_\phi\phi + F_y h\mathbf{c}_\phi + mgh\mathbf{s}_\phi + M_x & (2.10) \\ \tau_z &= -F_x h\mathbf{s}_\phi + M_z & (2.11) \end{aligned}$$

where F_x, F_y, and M_z are the total longitudinal and lateral forces and yaw moment applied to the vehicle at the tire contact patches. M_x in this context is an actuated roll moment from the suspensions, to be controlled. Usually, we can estimate the longitudinal and lateral forces by their respective accelerations, i.e. as d'Alembert forces $F_x \approx ma_x$ and $F_y \approx ma_y$. Combining everything together yields the coupled nonlinear ODEs

$$\begin{aligned} I_{xx}\ddot{\phi} - \dot{\psi}^2 (I_{yy} - I_{zz})\,\mathbf{c}_\phi\mathbf{s}_\phi + c_\phi\dot{\phi} + k_\phi\phi - ma_y h\mathbf{c}_\phi - mgh\mathbf{s}_\phi &= M_x & (2.12) \\ \left(I_{zz}\mathbf{c}_\phi^2 + I_{yy}\mathbf{s}_\phi^2\right)\ddot{\psi} + 2\dot{\psi}(I_{yy} - I_{zz})\,\mathbf{c}_\phi\mathbf{s}_\phi + ma_x h\mathbf{s}_\phi &= M_z & (2.13) \end{aligned}$$

which fully describe the angular motion of the vehicle body. In this thesis, we will make use of the roll equation of motion to design a control law for the actuated moment M_x.

Remark. *From these equations we can see that the roll and yaw degrees of freedom are significantly coupled. We will focus primarily on control using suspensions, however we note that the roll dynamics can be improved also by designing a suitable yaw controller for M_z, which is the task of ESC design.*

Remark. *Strictly speaking, the above equations depend on the translational dynamics through the longitudinal and lateral accelerations. For control purposes, it suffices to have an online estimate of these quantities from sensors, thus we do not need to derive the translational dynamic equations. The interested reader may find a derivation of the translational dynamics in [18].*

Model Validity and Vehicle Rollover

The two-track model of a ground vehicle contains a built-in assumption: that all tire of the vehicle remain constrained to the ground. When this ceases to be the case, dynamic effects of the suspensions become less important and vehicle rollover becomes imminent. This leads us to the concept of *lateral load transfer*. A common quantification of load transfer is the *rollover index*

$$\mathrm{RI} = \frac{F_R - F_L}{F_R + F_L} \tag{2.14}$$

where F_R and F_L are the tire forces on the right and left-hand sides of the vehicle, respectively. The rollover index takes on a value of ± 1 when the normal forces on either side of the vehicle become zero, which indicates wheel lift-off.

For stability, it is imperative to design a system which stabilizes the lateral load transfer in order to prevent rollover. Controlling load transfer has other benefits as well, particularly in improving vehicle handling. This is because the dynamic normal force at the tire determines the longitudinal and lateral forces at the contact patch, in other words, controlling the variation of the normal force improves traction at the wheels. Many approximations to the rollover index exist in the literature, and these tend to be functions of the lateral acceleration a_y, the roll angle ϕ and the roll rate $\dot{\phi}$. It can be shown via straightforward static analysis that

$$\mathrm{RI} = \frac{k_\phi \phi + c_\phi \dot{\phi}}{mg} \tag{2.15}$$

where m is the total mass of the vehicle and g is the gravity constant. Thus, regulating lateral load transfer reduces to regulating roll angle and roll rate, which together constitute the suspension roll moment.

2.1.2 Quarter-Car Model

By far, the most common model considered in the design and control of suspensions is the quarter-car model. The model consists of two masses: the sprung mass m_s representing the vehicle body and the unsprung mass m_u representing the mass of a single tire. The tire stiffness is represented by a linear spring, and the suspension itself is a combination of a linear spring and damper in parallel between the sprung and unsprung masses.

In contrast to the two-track vehicle model, the quarter-car model is used to analyse the characteristics of a vehicle's vibrational modes. The quarter-car model is a linear system, which calls for a different set of techniques for analysis than the nonlinear models of the previous section. In passive suspension design, as well as in the design of suspension control systems, the natural frequencies and damping ratios of the quarter-car model are shaped to desired design specifications to achieve a certain performance objective.

Here, we derive the equations of motion of the quarter-car model with passive damping and control input using the Lagrangian formalism. The potential and kinetic energy and dissipation functions of the quarter-car model are given by

$$T = \frac{1}{2}m_s\dot{z}_s^2 + \frac{1}{2}m_u\dot{z}_u^2 \tag{2.16}$$

$$V = \frac{1}{2}k\left(z_s - z_u\right)^2 + \frac{1}{2}k_t\left(z_u - r\right)^2 \tag{2.17}$$

$$D = \frac{1}{2}c\left(\dot{z}_s - \dot{z}_u\right)^2 \tag{2.18}$$

where r is a disturbance at the road surface. Defining the state variables $q = [z_s, z_u]^T$, the equations of motion for the system are given by Lagrange's equation

$$\frac{d}{dt}\frac{\partial T}{\partial \dot{q}} - \frac{\partial T}{\partial q} + \frac{\partial V}{\partial q} + \frac{\partial D}{\partial \dot{q}} = Q \tag{2.19}$$

where Q is a vector of generalized forces. The partial derivatives of T, V, and D with respect to q and $\dot{q}$ are

$$\frac{\partial T}{\partial \dot{q}} = \begin{bmatrix} m_s\dot{z}_s \\ m_u\dot{z}_u \end{bmatrix} \tag{2.20}$$

$$\frac{\partial T}{\partial q} = 0 \tag{2.21}$$

$$\frac{\partial V}{\partial q} = \begin{bmatrix} k\left(z_s - z_u\right) \\ -k\left(z_s - z_u\right) + k_t\left(z_u - r\right) \end{bmatrix} \tag{2.22}$$

$$\frac{\partial D}{\partial \dot{q}} = \begin{bmatrix} c\left(\dot{z}_s - \dot{z}_u\right) \\ -c\left(\dot{z}_s - \dot{z}_u\right) \end{bmatrix} \tag{2.23}$$

and the generalized force vector Q is obtained from the expression for virtual work

$$\delta W = \sum_{i=0}^{2} Q_i \delta q_i = u\delta z_s - u\delta z_u \tag{2.24}$$

where u is the actuated force at the suspensions. Q has the form

$$Q = \begin{bmatrix} u \\ -u \end{bmatrix}. \tag{2.25}$$

Substituting these quantities into Lagrange's equation yields the ODE system

$$\begin{aligned} m_s\ddot{z}_s + c\left(\dot{z}_s - \dot{z}_u\right) + k\left(z_s - z_u\right) &= u & (2.26)\\ m_u\ddot{z}_u - c\left(\dot{z}_s - \dot{z}_u\right) - k\left(z_s - z_u\right) + k_t\left(z_u - r\right) &= -u. & (2.27) \end{aligned}$$

2.1.3 Half-Car and Full-Car Models

The final vehicle models we will consider in this thesis are the *half-car* and *full-car* models. These models consist of a sprung mass m_s suspended by linear springs and dampers at multiple points. That is, the half-car model is essentially two quarter-car models connected to a single sprung mass, representing half of the vehicle body. Likewise, the full-car model is a combination of four quarter-car models attached to the same sprung mass.

Half-Car Model

The half-car model enables us to model the pitch and vertical motion of a ground vehicle, while ignoring roll and other motions. As such, the half-car is a fitting complement to the two-track vehicle model, as together they cover all six degrees of freedom of the vehicle system. Like the quarter-car, the half-car model is a linear system. This is principally because the pitch angle θ of a ground vehicle is usually sufficiently small in magnitude to justify applying a small angle approximation.

Unlike with roll, pitch dynamics have little to do with vehicle stability, but like purely vertical vibrations, have a lot to do with ride comfort. Thus, it makes intuitive sense to apply a model which can describe both the pitch and vertical sprung mass motions simultaneously, as we will be applying the same control design techniques to both degrees of freedom.

As with the quarter-car model, we derive the equations of motion for the half-car model using the Lagrangian formalism. The following derivation and discussions of these models can be found in various books on vehicle dynamics and modeling, for example in [13, 26]. The potential and kinetic energy and dissipation functions of the half-car model are given by

$$T = \frac{1}{2}m_s\dot{z}_s^2 + \frac{1}{2}m_{u_1}\dot{z}_{u_1}^2 + \frac{1}{2}m_{u_2}\dot{z}_{u_2}^2 + \frac{1}{2}I_{yy}\dot{\theta}^2 \tag{2.28}$$

$$V = \frac{1}{2}k_1\left(z_s + a\mathbf{s}_\theta - z_{u_1}\right)^2 + \frac{1}{2}k_2\left(z_s - b\mathbf{s}_\theta - z_{u_2}\right)^2 + \frac{1}{2}k_{t_1}z_{u_1}^2 + \frac{1}{2}k_{t_2}z_{u_2}^2 \tag{2.29}$$

$$D = \frac{1}{2}c_1\left(\dot{z}_s + a\mathbf{s}_\theta - \dot{z}_{u_1}\right)^2 + \frac{1}{2}c_2\left(\dot{z}_s - b\mathbf{s}_\theta - \dot{z}_{u_2}\right)^2. \tag{2.30}$$

Defining states $q = [z_s, \theta, z_{u_1}, z_{u_2}]^T$, the equations of motion for the system are given by Lagrange's equation

$$\frac{d}{dt}\frac{\partial T}{\partial \dot{q}} - \frac{\partial T}{\partial q} + \frac{\partial V}{\partial q} + \frac{\partial D}{\partial \dot{q}} = Q \tag{2.31}$$

where Q is a vector of generalized forces, obtained from the expression for virtual work

$$\delta W = \sum_{i=0}^{4} Q_i \delta q_i = (u_1 + u_2)\delta z_s + (au_1 - bu_2)\delta\theta - u_1\delta z_{u_1} - u_2\delta z_{u_2} \tag{2.32}$$

where u_1 and u_2 are the actuated forces at the front and rear suspensions, respectively. Q has the form

$$Q = \begin{bmatrix} u_1 + u_2 \\ au_1 - bu_2 \\ -u_1 \\ -u_2 \end{bmatrix}. \tag{2.33}$$

Applying the small angle approximation $\mathbf{s}_\theta \approx \theta$, we obtain the matrix ODE

$$M\ddot{q} + C\dot{q} + Kq = Q \tag{2.34}$$

where

$$M = \begin{bmatrix} m_s & 0 & 0 & 0 \\ 0 & I_{yy} & 0 & 0 \\ 0 & 0 & m_{u_1} & 0 \\ 0 & 0 & 0 & m_{u_2} \end{bmatrix} \tag{2.35}$$

$$C = \begin{bmatrix} c_1 + c_2 & -ac_1 + bc_2 & -c_1 & -c_2 \\ -ac_1 + bc_2 & c_1a^2 + c_2b^2 & ac_1 & -bc_2 \\ -c_1 & ac_1 & c_1 & 0 \\ -c_2 & -bc_2 & 0 & c_2 \end{bmatrix} \tag{2.36}$$

$$K = \begin{bmatrix} k_1 + k_2 & -ak_1 + bk_2 & -k_1 & -k_2 \\ -ak_1 + bk_2 & k_1a^2 + k_2b^2 & ak_1 & -bk_2 \\ -k_1 & ak_1 & k_1 + k_{t_1} & 0 \\ -k_2 & -bk_2 & 0 & k_2 + k_{t_2} \end{bmatrix} \tag{2.37}$$

are the mass, damping, and stiffness matrices, respectively. The above system model has four degrees of freedom, two for the sprung mass and one for each of the two unsprung masses. This model can be reduced to a two degree of freedom model by simply removing the last two rows and columns of each matrix. Such a reduced model is studied extensively by Wong in [26]. The reduced model contains only information about the sprung mass dynamics whereas the full four degree of freedom model contains the dynamics of the front and rear wheels as well. In this thesis, our focus is primarily on sprung mass dynamics, thus we will make use of the two degree of freedom model for control design. When refering to the reduced model, we will use the same notation for the equation of motion as above.

For our control design, instead of the front and rear suspension actuations, we would like our control variables to be the generalized pitch moment M_y and vertical force F_z on the sprung mass. These quantities are defined by the equations

$$M_y = au_1 - bu_2 \tag{2.38}$$

$$F_z = u_1 + u_2. \tag{2.39}$$

Thus, we may write

$$M\ddot{q} + C\dot{q} + Kq = \begin{bmatrix} F_z \\ M_y \end{bmatrix} \tag{2.40}$$

With the aforementioned states and system matrices, we now have a suitable model for control design using the generalized pitch moment M_y and vertical force F_z.

Full-Car Model

The full-car model is a natural extension of the quarter-car and half-car models to include vertical motion, pitch, *and* roll of the sprung mass. Each quarter-car represents one of the four vehicle suspensions. The model is linear, due to imposing a small angle approximation on the roll degree of freedom as well as the pitch degree of freedom. As such, the full-car model is less accurate in modeling the roll motion as roll angle increases. Moreover, since the nonlinear coupling between the yaw rate and lateral acceleration is ignored in the equations of motion, the full-car model does not give a complete description of the phenomena influencing the roll dynamics. For these reasons, we will not use the full-car model for control design, however we have mentioned it here for completeness. The interested reader can find the full derivation of the equations of motion in [13].

2.2 Suspension Control

2.2.1 Active Systems

Active suspension systems have been and remain an area of active research in the automotive and control community for over two decades, though they have to date not been widely commercialized. These systems are characterized by their ability to both inject and dissipate power in the suspensions. This makes designing a controller using the popular optimal control methods, e.g. LQR, LQG, H_∞, etc. comparatively simple, as the actuators are not constrained to only dissipate power, as in semi-active systems.

The most famous example of an actual active suspension system is that in development by Bose Corporation since 1980 [6, 15]. The Bose suspension system uses linear electromagnetic actuators at each corner in place of passive dampers and torsion bars to suspend the vehicle. Moreover, each actuator can be independently controlled in order to optimize handling and ride. Despite its long development period, the Bose suspension is not yet present in production vehicles, likely due to prohibitively high costs and power requirements. Other active systems include the Active Body Control (ABC) system by Mercedes-Benz [1] and the Dynamic Drive System by BMW [22]. In constrast to the Bose system, both ABC and Dynamic Drive consist of hydraulic rather then electromagnetic actuators. The Dynamic Drive system in particular is actually an active stabilizer bar system rather than a set of independent actuators. As such, the mechanism is designed to optimize roll angle.

2.2.2 Semi-active Systems

Semi-active suspension systems are characterized by their ability to only dissipate power in the suspensions. As such, semi-active suspensions must obey a so-called *passivity constraint*, which is that semi-active actuators can only exert force opposite their direction of motion.

The canonical example of a semi-active actuator is a *magnetorheological* (MR) damper. MR dampers, also known as variable dampers, contain a rheological fluid whose stiffness is proportional to the strength of the magnetic field through its volume. MR dampers function by inputing a specified electrical current, which by virtue of flowing through a solenoid coil, manipulate the magnetic field within the damper, causing the fluid within to change its viscous damping properties accordingly. When the magnetic field strength is high, the iron particles suspended in the fluid align along the magnetic field lines, which causes the fluid to become more viscous and semi-solid. When the magnetic field strength is low, the fluid returns to a state of lower viscosity. Advantages of semi-active control using MR dampers include low power requirements, relatively cheap implementation, and high actuator bandwidth. A popular semi-active control system using MR dampers is the MagneRide system by BWI Group, available on many commercial vehicles.

Control of semi-active suspension systems can be viewed as either varying actuator force given certain upper and lower limits, or varying the damping properties of the system. In this work, we formulate control laws in terms of actuator forces. Below, we survey some common implementations of semi-active control. All of the following control strategies originate from analysis and design on a quarter-car model. An extensive survey of semi-active control methodologies is given by Poussot-Vassal, et al. in [17].

Skyhook Control

Skyhook control is a control strategy specifically designed to dampen motion of the sprung mass, i.e. to improve ride comfort. The derivation of the skyhook control involves finding a control law which emulates a fictitious linear damper with coefficient C_{sky} connected to the sprung mass and a reference point usually depicted as in the sky, hence the name. The skyhook control law is given by

$$F_{sky}(\dot{z}_s, \dot{z}) = \begin{cases} -C_{sky}\dot{z}_s & \text{if } \dot{z}_s\dot{z} > 0 \\ 0 & \text{if } \dot{z}_s\dot{z} < 0 \end{cases} \tag{2.41}$$

where $\dot{z}_s$ is the vertical velocity of the sprung mass and $\dot{z}$ is the velocity of the suspension, defined by $\dot{z} = \dot{z}_s - \dot{z}_u$.

Groundhook Control

Groundhook control is a control strategy specifically designed to dampen motion of the wheel, i.e. the unsprung mass. The goal of groundhook control is to lessen variation in the dynamic tire force, which improves the handling properties of the vehicle. The derivation of the groundhook control, similar to skyhook, involves finding a control law which emulates a fictitious linear damper with coefficient C_{gnd} connected to the unsprung mass and a reference point on the ground. The groundhook control law is given by

$$F_{gnd}(\dot{z}_s, \dot{z}) = \begin{cases} -C_{gnd}\dot{z}_u & \text{if } \dot{z}_u\dot{z} < 0 \\ 0 & \text{if } \dot{z}_u\dot{z} > 0 \end{cases} \tag{2.42}$$

where $\dot{z}_u$ is the vertical velocity of the unsprung mass and $\dot{z}$ is the velocity of the suspension.

Hybrid Control

The *hybrid control* strategy, as the name suggests, blends the skyhook and groundhook laws to produce a controller which improves both ride comfort and handling. The hybrid control law is defined by

$$F_{hyb} = \alpha F_{sky} + (1 - \alpha) F_{gnd} \tag{2.43}$$

where $\alpha \in [0, 1]$ is a constant. Clearly, a value of $\alpha = 1$ signifies pure skyhook control, and a value of $\alpha = 0$ signifies pure groundhook control. Various design criteria exist for choosing an intermediate α which blends the skyhook and groundhook effects. The blending parameter α can also be designed to vary situationally for adaptive control. In particular, an adaptive algorithm for hybrid control of semi-active suspensions is given by Agrawal and Khajepour in [2, 3], which will provide some inspiration for the sections on adaptivity.

Clipped Optimal Control

Another method of semi-active control, slightly different from the three methods above, is to design a control law assuming an active actuator using optimal control methods and "clipping" it by imposing the passivity constraint. The control law F_a for the active system can be computed using well-known techniques such as LQR, LQG, or H_∞, among others, and applying the passivity constraint, one obtains

$$F_{sa} = \begin{cases} F_a & \text{if } \dot{z}_s\dot{z} > 0 \\ 0 & \text{if } \dot{z}_s\dot{z} < 0 \end{cases} \tag{2.44}$$

2.3 Optimization and Control Allocation

2.3.1 Control Allocation

Now that we have introduced the vehicle models of interest and the common methods of suspension control, we will turn our attention to the subject of *control allocation*. Control allocation is a relatively new area of control systems research which has emerged over the course of the last couple decades, which has been and continues to find new applications in numerous areas of research ranging from automotive systems, aerospace, marine systems, and robotics. Control allocation techniques have high utility when designing systems which are overactuated, hence their applications in flight controls and growing prominence in the automotive sector.

The general structure of a control system designed with the control allocation methodology is divided into two distinct parts: the high-level controller and the control allocator. The control signals generated by the high-level controller are referred to as the *virtual control signals*, so-called because these control signals need not correspond to any one physical actuator. In the context of vehicle dynamics controllers, in either automotive or aerospace domains, the virtual signals correspond to generalized forces and moments applied to the vehicle CG. The control allocator, as the name suggests, is to distribute the control actions produced by the high-level controllers among the available actuators physically present in the system.

The control allocation module is typically defined as an optimization problem, in which case we may refer to the process as *optimal control allocation*. The central objective of the allocation task is to minimize the *control allocation error*, which is the difference between the virtual control signal and the combined effort of the actuators. If we denote by $v \in \mathcal{V}$ the virtual controls, and by $u \in \mathcal{U}$ the actuator efforts, then typically we can find a mapping $h : \mathcal{U} \to \mathcal{V}$ called an *effector model* which relates the actuator efforts to the virtual controls. In general, this mapping can be static, time-varying, state-dependent, linear or nonlinear. The control allocation error is then defined as the quantity $v - h(u)$. In the case that the effector model is a linear mapping, it is often referred to as the *control effectiveness matrix* of the system, and denoted by B.

Depending on the preferences of the designer, the defining optimization problem of the control allocation can be either linear, quadratic, generally convex, or generally nonlinear in form. In part, this is determined by the chosen effector model h, but also by the overall structure of the objective function, and of the constraints defining the feasible actuations $\mathcal{U}$. In this work, we restrict ourselves to the case of a linear effector model, a quadratic

objective function, and linear constraints. This formulation is sometimes referred to as *constrained quadratic control allocation*, but in general can be thought of as a quadratic programming problem with linear constraints.

The primary objective of the control allocation, as stated before, is to minimize the control allocation error. Given the set of feasible control actions $\mathcal{U} \subset \mathbb{R}^n$, the quadratic control allocation problem has the following formulation:

$$\min_{u \in \mathcal{U}} \quad \frac{\gamma}{2} \|v - Bu\|_{W_v}^2 + \frac{1}{2} \|u - u_0\|_{W_u}^2 \tag{2.45}$$

where v are the virtual control signals, u are the actuator signals, $u_0 \in \mathbb{R}^n$ is a given vector, $\gamma \in \mathbb{R}$, $W_v, W_u > 0$ are positive definite weighting matrices and $\|x\|_W = (x^T W x)^{1/2}$ denotes the L^2-norm weighted by W. On account of the use of the L^2-norm, this setup is sometimes referred to as L^2-*optimal control allocation*. With this form of objective function, the optimal solution is a compromise between minimizing the control allocation error, and the deviation of the actuations from some specified equilibrium point u_0. The relative importance of either objective is controllable by designing the weighting matrices W_v, W_u and the parameter γ appropriately. It can be shown that as the parameter $\gamma \to \infty$, the solution of the QP problem (2.45) approaches the solution of the sequential least-squares (SLS) formulation

$$\begin{aligned} \min_{u \in \Omega} \quad & \|u - u_0\|_{W_u} \\ \text{s. t.} \quad & \Omega = \arg\min_{u \in \mathcal{U}} \|v - Bu\|_{W_v} \end{aligned} \tag{2.46}$$

which minimizes the control allocation error with first priority, followed by the deviation from equilibrium. Thus, the quadratic control allocation can functionally solve for the same optimal control distribution as the more explicit SLS formulation, while at the same time enabling efficient computation using contemporary numerical methods designed for solving quadratic programs.

Advantages of the control allocation approach to control system design include straightforward implementation of actuator constraints, adaptivity and fault tolerance. The use of an optimization process to minimize the control allocation error ensures that the actuator efforts match the virtual control as well as possible. Secondary objectives can be easily incorporated into the control strategy by modifying various aspects of the objective function. We will revisit these ideas later in the sections on control allocator design.

The research herein can be viewed as a continuation of that presented by Schofield and Hägglund in [18, 19, 20, 21] where control allocation via quadratic programming was used for simultaneous yaw stabilization and rollover detection and prevention using an

active braking system. Schofield's research is an application of the more general theory of constrained quadratic control allocation explored by Härkegård in [11], where application of the subject to flight controls was also covered. In [10], Härkegård formulated an active-set method for solution of the quadratic control allocation problem. Härkegård generalized the quadratic control allocation paradigm to include compensation for actuator dynamics in [12].

Other applications of control allocation techniques in vehicle dynamics research include the study by Wang and Wang [25] where quadratic control allocation was used with torque vectoring for fault tolerant stability control of a 4WD electric vehicle. Nonlinear programming methods in control allocation have been used as well for the design of ESC systems, for example by Tøndel, Tjønnås, and Johansen in [23, 24]. .

Control allocation as a subject is diverse and covers many other formulations than the quadratic case applied in this work. Moreover, the subject is continually finding new applications. Those interested in a survey of control allocation methods and their applications may see [14].

2.3.2 Quadratic Programming

Quadratic programming is the study of problems involving minimizing (or maximizing) a quadratic objective function. Letting $x \in \mathbb{R}^n$ denote the vector of decision variables to be solved for, quadratic minimization problems have the form

$$\begin{aligned} \min_{x \in \mathbb{R}^n} \quad & x^T H x + g^T x \\ \text{s. t.} \quad & Ax \leq b \end{aligned} \tag{2.47}$$

where H is a symmetric, positive definite matrix called the *Hessian*, g is a vector called the *gradient*, and the linear matrix inequality $Ax \leq b$ defines the region of feasible solutions. Quadratic programming is a well-studied topic, and many algorithms exist for solving quadratic programs of various sizes, either online or offline. Most of these can be classed as certain types of algorithms like active-set methods, interior point methods, gradient methods, etc. When the problem is unconstrained and H is nonsingular, then a closed-form solution exists which can be derived via straightforward differential calculus. It is given simply by

$$x^* = -\frac{1}{2} H^{-1} g. \tag{2.48}$$

More generally, solutions of quadratic programs, by virtue of the latter being a special case of *convex* programs, are guaranteed to exist provided that the set of feasible solutions

defined by the constaints is itself a convex set. For constrained problems, however, closed-form expressions of these solutions are not guaranteed to exist, hence the need for an algorithmic solver.

For online computation, as required for constrained quadratic control allocation, active-set methods are preferable because they are relatively fast and have the property that each iteration of the algorithm produces a feasible suboptimal solution. A couple contemporary solvers that use active-set methods and which have been previously employed in online optimization are `qpOASES`[1] developed by Ferreau in [7] and `QCAT`[2] (Quadratic Control Allocation Toolbox) by Härkegård in [9, 10].

The basic idea behind active-set methods is that at each iteration, a subset of the inequality constraints are taken to be equality constraints and the rest are ignored. The set of constraints $\mathcal{W}$ which are "active" is termed the *working set*. The optimization is then performed on this set to find the optimal perturbation p from the current suboptimal solution u^i. This generates a new suboptimal solution $u^{i+1} = u^i + p$. If u^{i+1} is feasible, then the solution is checked for optimality by looking at the Lagrange multipliers. If the solution is found to be optimal, then the algorithm terminates, else the working set $\mathcal{W}$ is updated with new active constraints and the algorithm begins a new iteration.

For the experiments documented in this work, the `QCAT` toolbox was used for online optimization on a dSPACE AutoBox. The algorithm, as formulated by Härkegård in [10] is reproduced here for reference. Härkegård noted that the quadratic objective function in (2.45) may be rewritten as

$$\frac{\gamma}{2}\left\|v - Bu\right\|_{W_v}^2 + \frac{1}{2}\left\|u - u_0\right\|_{W_u}^2 = \frac{1}{2}\underbrace{\left\|\begin{pmatrix}(\gamma W_v)^{\frac{1}{2}} B \\ W_u^{\frac{1}{2}}\end{pmatrix} u - \begin{pmatrix}(\gamma W_v)^{\frac{1}{2}} v \\ W_u^{\frac{1}{2}} u_0\end{pmatrix}\right\|^2}_{=:\|Au-b\|^2}. \tag{2.49}$$

Supposing that the set of feasible solutions $\mathcal{U}$ is described by box constraints, i.e. we have $\underline{u}_i \leq u_i \leq \bar{u}_i$, then the quadratic program reduces to solving

$$\begin{aligned} \min_{u\in\mathbb{R}^n} \quad & \|Au - b\| \\ \text{s. t.} \quad & \underbrace{\begin{pmatrix} I \\ -I \end{pmatrix}}_{=:C} u \leq \begin{pmatrix} \overline{u} \\ -\underline{u} \end{pmatrix} \end{aligned} \tag{2.50}$$

[1] `http://set.kuleuven.be/optec/Software/qpOASES-OPTEC`
[2] `http://research.harkegard.se/qcat/index.html`

which can be solved efficiently using Algorithm 1 below.

Those interested in the theory and application of convex optimization (including quadratic programming) may see the text [5] by Boyd and Verdenberghe, which is freely available online from the authors[3].

[3]http://www.stanford.edu/ boyd/cvxbook/

Input: A feasible initial iterate u^0.
Output: The optimal control distribution u^*.
for $i = 0, 1, 2, ...$ **do**
    Given the suboptimal iterate u^i and the working set of active constraints $\mathcal{W}$, solve the following equality constrained problem for the optimal perturbation p:

$$\begin{aligned} \min_{p \in \mathbb{R}^n} \quad & \left\| A(u^i + p) - b \right\| \\ \text{s. t.} \quad & \begin{aligned} Bp &= 0 \\ p_j &= 0, \qquad \forall j \in \mathcal{W} \end{aligned} \end{aligned} \tag{2.51}$$

    if $u^i + p$ *is feasible* **then**
        Set $u^{i+1} = u^i + p$;
        Compute the Lagrange multipliers λ, μ via

$$A^T \left(Au^{i+1} - b \right) = \begin{pmatrix} B^T & C_i^T \end{pmatrix} \begin{pmatrix} \mu \\ \lambda \end{pmatrix} \tag{2.52}$$

        where C_i is the matrix formed by the rows of C corresponding to constraints in the working set $\mathcal{W}$ for the current iteration;
        if $\lambda \geq 0$ **then**
            The optimal solution has been found;
            return $u^* = u^{i+1}$;
        else
            Remove the constraint corresponding to the most negative Lagrange multiplier λ from the working set $\mathcal{W}$;
        end
    end
end

Algorithm 1: `QCAT` active-set algorithm.

□

Chapter 3

Design and Simulation

3.1 High-Level Controller Design

In the following two chapters, we present the design, simulation, implementation, and experimentation of the coordinated suspension control system, or CSC. We begin by developing the high-level controllers for the roll, pitch and vertical motions of the vehicle. As explained in the previous chapter, our approach to coordinated suspension control uses these high-level controllers to generate the virtual control signals, e.g. the roll and pitch moments M_x and M_y and the vertical CG force F_z, which the actuators must work together to exert on the vehicle body. For this, we apply techniques from both nonlinear and advanced linear control theory, namely sliding mode control (SMC).

Sliding mode control is a nonlinear control technique which guarantees asymptotic stability of the closed loop system even in the presence of modeling errors. This is particular useful, since the vehicle dynamics are nonlinear in nature and parametric uncertainties can have a large impact on the system behavior. The use of sliding mode control thus enables us to take these nonlinear behaviors into account, which is particularly important at high speeds and in harsh maneuvers. For general background on nonlinear control theory and sliding mode control in particular, the interested reader may see [16].

3.1.1 Roll Control

The roll dynamics of the ground vehicle may be represented by the two-track model. Recall that the nonlinear angular dynamic equation of motion for the roll degree of freedom is

given by

$$I_{xx}\ddot{\phi} - \dot{\psi}^2 \left(I_{yy} - I_{zz}\right) \mathbf{c}_\phi \mathbf{s}_\phi + c_\phi \dot{\phi} + k_\phi \phi - m a_y h \mathbf{c}_\phi - mgh\mathbf{s}_\phi = M_x. \tag{3.1}$$

Here, we design a sliding mode controller using the generalized moment M_x as the control variable. The system (3.1) may be rewritten as

$$\ddot{\phi} = f(\phi, \dot{\phi}, \dot{\psi}, a_y) + \frac{1}{I_{xx}} M_x \tag{3.2}$$

where

$$f(\phi, \dot{\phi}, \dot{\psi}, a_y) = \frac{1}{I_{xx}} \left(-k_\phi \phi - c_\phi \dot{\phi} + m a_y h \mathbf{c}_\phi + mgh\mathbf{s}_\phi + \dot{\psi}^2 \left(I_{yy} - I_{zz}\right) \mathbf{c}_\phi \mathbf{s}_\phi \right).$$

Our control objective is to drive the roll motion to zero state. To this end, define the sliding manifold

$$s = \dot{\phi} + \lambda \phi = 0 \tag{3.3}$$

for some $\lambda > 0$, which implies that the sliding manifold defines stable dynamics. We seek a control law which drives the system to the sliding manifold. Let

$$M_x = k_\phi \phi + c_\phi \dot{\phi} - m a_y h \mathbf{c}_\phi - mgh\mathbf{s}_\phi - \dot{\psi}^2 \left(I_{yy} - I_{zz}\right) \mathbf{c}_\phi \mathbf{s}_\phi - I_{xx} \left(\lambda \dot{\phi} + k \mathrm{sgn}(s) \right). \tag{3.4}$$

The asymptotic stability of the sliding surface can be proved using Lyapunov's direct method, as in [16].

Proposition 1 (Stability of the Roll SMC)**.** *The control law* (3.4) *stabilizes the sliding manifold* (3.3) *in finite time and asymptotically stabilizes the origin.*

Proof. We define the Lyapunov function candidate

$$V = \frac{1}{2} s^2. \tag{3.5}$$

Differentiation with respect to time gives

$$\begin{aligned} \dot{V} &= s\dot{s} && (3.6)\\ &= s\left(\ddot{\phi} + \lambda \dot{\phi}\right) && (3.7)\\ &= s\left(f(\phi, \dot{\phi}, \dot{\psi}, a_y) + \frac{1}{I_{xx}} M_x + \lambda \dot{\phi} \right). && (3.8) \end{aligned}$$

To ensure stability of the sliding manifold $s = 0$, we require that $\dot{V} < 0$ such that (3.5) is a Lyapunov function for (3.1) and so that the system will reach the sliding surface in finite time. Therefore, choose $k > 0$ and let

$$M_x = -I_{xx}\left(f(\phi, \dot{\phi}, \dot{\psi}, a_y) + \lambda\dot{\phi} + k\text{sgn}(s)\right) \tag{3.9}$$

then it follows that

$$\begin{aligned} \dot{V} &= -ks\text{sgn}(s) && (3.10)\\ &= -k\,|s| && (3.11)\\ &< 0 && (3.12) \end{aligned}$$

as desired. On the sliding manifold $s = 0$, the roll dynamics reduce to the first order linear system $\dot{\phi} = -\lambda\phi$, which converges exponentially to zero with rate λ. Hence, the controller (3.4) asymptotically stabilizes the origin. □

Remark. *We must be wary of the above stability result. The model for roll motion which we used to design the control law is only valid when both wheels of the vehicle remain on the ground. When the lateral load transfer reaches a critical value, or equivalently, when the roll angle exceeds a certain limit, then the dynamics change and the suspensions are no longer viable for roll control. Nevertheless, we can conclude that for as long as the vehicle satisfies this operating condition, then the controller* (3.4) *is asymptotically stable.*

The controller (3.4) can be viewed as a superposition of various parts. The terms involving the lateral acceleration a_y and the yaw rate $\dot{\psi}$ can be thought of as feedforward components for disturbance rejection. The switching function $k\text{sgn}(s)$ ensures that for sufficiently large $k > 0$, the system evolves towards the sliding surface even with the presence of model errors, for instance, variations in the mass parameter m or uncertainty in the distance from the roll center h, which can be difficult to measure and varies to an extent during operation.

The use of the discontinuous sgn function does however lead to a chattering effect about the sliding manifold. In practical implementation, this can be reduced by replacing the sgn function with a saturation function, which deactivates the term within a boundary layer of specified width. Such a saturation function has the form

$$\text{sat}(s) = \begin{cases} \frac{s}{\varepsilon} & \text{for } |s| < \varepsilon \\ 1 & \text{for } s \geq \varepsilon \\ -1 & \text{for } s \leq -\varepsilon \end{cases}$$

where $\varepsilon > 0$ is the width of the boundary layer.

3.1.2 Pitch and Vertical Motion Control

As with the roll controller derived above, we design sliding mode controllers for the pitch and vertical degrees of freedom of the vehicle. For this design, we will apply the two degree of freedom half-car model to represent the dominant dynamics. Recall that the equation of motion of the half-car model is given by the matrix equation (2.40)

$$M\ddot{q} + C\dot{q} + Kq = \begin{bmatrix} F_z \\ M_y \end{bmatrix} \tag{3.13}$$

where the system states of interest are $q = [z_s, \theta]^T$ and the control inputs are given by $w = [F_z, M_y]^T$. Here, we design sliding mode controllers using these generalized efforts as the control variables. Rearranging (3.13), we have

$$\ddot{q} = -M^{-1}\left(Kq + C\dot{q} - w\right). \tag{3.14}$$

Defining the sliding manifold $\sigma = 0$ by the equation

$$\sigma = \dot{q} + \Lambda q = 0 \tag{3.15}$$

where $\Lambda > 0$ is a positive definite matrix. This implies that the spectrum of Λ is contained in the right half-plane, and so the sliding manifold defines stable dynamics. We seek a control law which drives the dynamics of the vehicle asymptotically to the sliding manifold. Let

$$\begin{bmatrix} F_z \\ M_y \end{bmatrix} = Kq + C\dot{q} - M^{-1}\left(\Lambda\dot{q} + \kappa\mathrm{sgn}(\sigma)\right) \tag{3.16}$$

where $\mathrm{sgn}(\sigma)$ is to be understood as the vector whose ith element is the ordinary signum function applied to the corresponding element of σ, and $\kappa > 0$ is a positive definite diagonal matrix.

As with the roll controller, the asymptotic stability of the sliding surface can be proved using Lyapunov's direct method, as in [16].

Proposition 2 (Stability of the Pitch and Vertical SMCs)**.** *The control law* (3.16) *stabilizes the sliding manifold* (3.15) *in finite time and asymptotically stabilizes the origin.*

Proof. We define the Lyapunov function candidate

$$V = \frac{1}{2}\sigma^T\sigma. \tag{3.17}$$

Differentiation with respect to time gives

$$\begin{aligned} \dot{V} &= \sigma^T \dot{\sigma} && (3.18)\\ &= \sigma^T \left(\ddot{q} + \Lambda \dot{q}\right) && (3.19)\\ &= \sigma^T \left(-M^{-1}\left(Kq + C\dot{q} - w\right) + \Lambda \dot{q}\right). && (3.20) \end{aligned}$$

To ensure stability of the sliding manifold $\sigma = 0$, we require that $\dot{V} < 0$ such that (3.17) is a Lyapunov function for (3.13) and so that the system will reach the sliding surface in finite time. Therefore, choose $\kappa = \text{diag}[k_1, k_2]$ for $k_1, k_2 > 0$ and let

$$w = Kq + C\dot{q} - M^{-1}\left(\Lambda \dot{q} + \kappa \text{sgn}(\sigma)\right) \tag{3.21}$$

then it follows that

$$\begin{aligned} \dot{V} &= -\sigma^T \kappa \text{sgn}(\sigma) && (3.22)\\ &= -k_1 \left|\sigma_1\right| - k_2 \left|\sigma_2\right| && (3.23)\\ &< 0 && (3.24) \end{aligned}$$

as desired. On the sliding manifold $\sigma = 0$, the system dynamics reduce to the first order linear system $\dot{q} = -\Lambda q$, which converges exponentially to zero. Hence, the controller (3.16) asymptotically stabilizes the origin. □

As with the roll controller, for sufficiently large gains $k_1, k_2 > 0$, the system evolves towards the sliding surface even with the presence of model errors, for instance, unmodeled nonlinearities, variations in the mass parameter m, or uncertainty in the suspension stiffness and damping properties. The chattering effect about the sliding manifold can likewise be alleviated with the use of a saturation function in place of the sgn function.

3.2 Control Allocator Design

In this section, we consider the task of distributing the virtual control action v, defined by the high-level controllers of the previous sections, over the available actuators on the vehicle, and given a set of admissible control actions $\mathcal{U} \subset \mathbb{R}^4$ defined by the actuator constraints. This is accomplished by solving an L^2-optimal control allocation problem by way of quadratic programming with linear constraints, which was briefly introduced in the previous chapter. The decision variables to be solved for are the actuator control signals,

which is to be done at each time step during operation. Specifically, we solve the following problem:

$$\min_{u \in \mathcal{U}} \quad \frac{\gamma}{2} \|v - Bu\|_{W_v}^2 + \frac{1}{2} \|u - u_0\|_{W_u}^2 \tag{3.25}$$

where $v = [M_x, M_y, F_z]^T$ are the virtual control signals, $u = [u_1, u_2, u_3, u_4]^T$ are the actuator signals, $u_0 \in \mathbb{R}^4$ is a given vector, $\gamma \in \mathbb{R}$, $W_v, W_u > 0$ are positive definite weighting matrices and $\|x\|_W = (x^T W x)^{1/2}$ denotes the L^2-norm weighted by W.

The purpose of the first term in the objective function (3.25) is to minimize the allocation error, i.e. the difference between the desired control action and the combined output of the actuators. In this context, $B : \mathcal{U} \to \mathcal{V}$ is the control effectiveness matrix, a linear mapping from the space of actuator signals into the space of virtual control signals. Specifically, B relates the lower-level controls to their output in terms of the generalized CG forces and moments.

The second term is meant to penalize deviation of the actuations from some given equilibrium state and to ensure convexity of the optimization problem, as in general, multiple solutions might exist such that $v = Bu$ on account of the overactuated nature of the system.

In the following sections, we elaborate on the setup of the control allocation problem. We derive the control effectiveness matrix and discuss appropriate actuator constraints for implementation with active and semi-active suspension systems.

3.2.1 Control Effectiveness Matrix

In this work, we restrict our attention to the vertical force actuations u on the sprung mass produced by four independent suspension actuators, either active or semi-active in nature. Assuming that the suspension forces always actuate perpendicularly to the plane of the sprung mass, the roll and pitch moments and the vertical force on the CG in terms of the suspension forces are given by

$$M_x = \frac{T}{2}(u_1 - u_2 + u_3 - u_4) \tag{3.26}$$

$$M_y = a\,(u_1 + u_2) - b\,(u_3 + u_4) \tag{3.27}$$

$$F_z = u_1 + u_2 + u_3 + u_4 \tag{3.28}$$

The control effectiveness matrix B is defined as the mapping relating the lower-level actuator controls to the virtual control signals v. Under these assumptions, the map is linear

and is given by

$$B = \begin{bmatrix} \frac{T}{2} & -\frac{T}{2} & \frac{T}{2} & -\frac{T}{2} \\ a & a & -b & -b \\ 1 & 1 & 1 & 1 \end{bmatrix}. \tag{3.29}$$

Implicitly, this design of the end effector map assumes that the angular motion of the sprung mass nor the geometric configuration of the suspensions affects the control allocation. In reality, the direction that the suspensions push and pull on the sprung mass change as the vehicle rolls and pitches and the suspensions themselves compress and extend. Thus, one might expect that the map B would be a function of the vehicle states. As such, it is reasonable to expect some error in the control allocation due to these approximations.

3.2.2 Active Systems

We now consider the design of the control allocation module for use with independent active suspensions. In the simplest case, i.e. assuming that the active suspensions are perfect actuators without constraints, then $\mathcal{U} = \mathbb{R}^4$ and the QP problem (3.25) has an analytical solution

$$u = \left(B^T W_v B + \frac{1}{\gamma} W_u\right)^{-1} \left(B^T W_v v - \frac{1}{\gamma} W_u u_0\right) \tag{3.30}$$

which can be derived using straightforward calculus. Furthermore, for active suspension systems, u_0 is usually taken to be zero, giving

$$u = \left(B^T W_v B + \frac{1}{\gamma} W_u\right)^{-1} B^T W_v v. \tag{3.31}$$

In practical situations we have constraints on the actuator outputs, that is we have box constraints $\underline{u}_i \leq u_i \leq \bar{u}_i$ for each i, possibly time or state-dependent, such that $\mathcal{U} = \prod_{i=1}^{4} [\underline{u}_i, \overline{u}_i]$. The QP problem to be solved is thus

$$\begin{aligned} \min_{u \in \mathbb{R}^4} \quad & \frac{\gamma}{2} \|v - Bu\|_{W_v}^2 + \frac{1}{2} \|u - u_0\|_{W_u}^2 \\ \text{s. t.} \quad & \underline{u} \leq u \leq \overline{u} \end{aligned} \tag{3.32}$$

Depending on the dynamics of the actuators in question, rate constraints might need to be defined as well. These can be easily realized by adding more linear constraints to the QP formulation.

In the case of constrained optimization, it is necessary to employ an online optimization algorithm for solution of the above QP in real time, such as an active-set or interior point method, since analytical solutions do not exist in general for constrained optimizations.

Remark. *Alternatively, the closed form solution* (3.31) *may be used with saturation to enforce the constraints, however optimality of the control allocation is not ensured in this case. Generally speaking, this is not advisable, as the QP problem is small enough dimensionally to allow for rapid solution and real-time implementation using active-set methods.*

3.2.3 Semi-active Systems

Having first considered the simpler case of fully active suspensions, we now turn our attention to the more complicated case of semi-active suspensions. We present an implementation of semi-active suspension control within the framework of optimal control allocation, using the QP constraints.

In the case of semi-active suspensions (MR dampers), we have the same type of QP problem as in (3.32), however the constaints on the actuators become essentially state-dependent. For semi-active control we require feedback of the suspension states to determine the minimum and maximum actuator outputs. Assuming that we have a static MR damper model $F_d = F_d(\dot{z}, i)$ to model the damping force, the minimum and maximum force output vectors $\underline{u}$ and $\overline{u}$ can be easily defined. The internal dynamics of MR dampers, being electromagnetic in nature, can be assumed to operate much faster than the mechanical motions of the suspensions. On this assumption, we can ignore rate constraints and define the upper and lower bounds on u by

$$\underline{u}_i = F_d(\dot{z}_i, i_{min}) \wedge F_d(\dot{z}_i, i_{max}) \tag{3.33}$$

$$\overline{u}_i = F_d(\dot{z}_i, i_{min}) \vee F_d(\dot{z}_i, i_{max}) \tag{3.34}$$

where $\wedge$ and $\vee$ denote the minimum and maximum elements, respectively, $\dot{z}_i$ is the suspension velocity at the ith wheel, i_{min} and i_{max} are minimum and maximum admissible currents to the dampers, respectively. In contrast to the active suspension, it is useful to take $u_0 = [u_{1,0}, u_{2,0}, u_{3,0}, u_{4,0}]^T$ where

$$u_{i,0} = F_d(\dot{z}_i, i_0) \tag{3.35}$$

for some baseline current input $i_0 \in [i_{min}, i_{max}]$. For the objective of minimizing the energy

consumption of the MR dampers, we take $i_0 = i_{min}$. The QP problem (3.25) thus becomes

$$\begin{aligned} \min_{u \in \mathbb{R}^4} \quad & \frac{\gamma}{2} \|v - Bu\|^2_{W_v} + \frac{1}{2} \|u - u_0\|^2_{W_u} \\ \text{s. t.} \quad & \underline{u}(\dot{z}) \leq u \leq \overline{u}(\dot{z}) \\ & u_0 = F_d(\dot{z}, i_0) \end{aligned} \tag{3.36}$$

where $\dot{z} = [\dot{z}_1, \dot{z}_2, \dot{z}_3, \dot{z}_4]^T$ and the objective function and constraints are dynamically updated at each time step in accordance with the suspension dynamics. As with the constrained active system, it is necessary to employ an online optimization algorithm for real-time solution of the QP problem. As state previously, active-set methods are well-suited to this task.

3.2.4 Adaptivity and Fault Tolerance

In this section, we turn our attention to the idea of making the above control allocation problem situationally adaptive. It makes intuitive sense that while driving, some situations would require roll control, such as taking a tight turn or making an evasive maneuver, whereas others would require pitch control, such as during periods of heavy acceleration and breaking. If we assume that the control system is fully active and unconstrained, then such an adaptation scheme is unnecessary, since the overactuation of the system ensures that both desired roll and pitch moments can always be applied to the vehicle. As soon as actuator constraints are brought into the picture, for example, with semi-active control, this ceases to be the case, and it would be advantageous to design criteria whereby roll control would be prefered and likewise for pitch control.

Additionally, there are situations where *decentralized* suspension control might be desirable in comparison to the centralized scheme afforded by the integrated system presented in the previous sections. For example, consider a vehicle driving straight at constant speed over a bumpy road. The roll and pitch vibrations, though extant, are not as large as they would be during intense maneuvering, so coordinated roll and pitch control are likely not necessary. Instead, the suspensions should be concentrating their efforts on the ride comfort objective, that is, controlling the sprung mass acceleration at each single corner, independently. As we shall see, by defining suitable adaptation parameters, the objective function of the control allocator module can be modified such that single-corner suspension control and coordinated roll and pitch control can be integrated into a single framework.

Finally, it is important that the control system is able to handle actuator failures. If one or more of the actuators malfunctions and becomes unusable, then the control allocation

problem should be modified to account for this failure and even suggest for the working actuators to compensate for the failure. All of this is possible within the framework of optimal control allocation.

Fault Tolerance

In the real world, things break under stress. If in extreme situations, the suspensions malfunction and cannot actuate forces correctly, the control allocation algorithm should be tuned such that the failed actuator is removed from the optimization process. This introduces yet another aspect of adaptivity and robustness in the control system, as the optimization process allows for the remaining actuators to compensate for system failures if they are able.

Fault tolerance can be achieved by modifying the control effectiveness matrix B and the vector u_0 in real time. If the ith actuator fails, then set the ith column of the matrix B and the ith element of u_0 to zero. This ensures that $u_i = 0$ and removes the failed actuator from consideration in the control allocation problem.

Adaptation Parameters

Here, we seek to define parameters α_{M_x} and α_{M_y} which quantify the need for roll and pitch control, respectively. For this, we must first analyze qualitatively when coordinated roll and pitch control are justified.

As stated at the beginning of this section, roll control is useful in extreme maneuvering, when cornering and when making evasive maneuvers. For the roll adaptation, we can take inspiration from rollover detection and prevention systems in the literature, which define a threshold roll angle $\hat{\phi}$ after which the control system activates. Ideally, however, we would like to include some predictive action into the adaptation process. For this, we can use as well the lateral acceleration a_y for adaptation. As with the roll angle, we may define a threshold a_y such that when the lateral acceleration exceeds this amount, the control system activates roll control for improved cornering.

As in the figure, the inputs to the adaptation scheme are the roll angle ϕ and the lateral acceleration a_y. First, both signals are normalized by their threshold values $\hat{\phi}$ and $\hat{a}_y$. The roll threshold is chosen to be roughly half of the so-called critical roll angle ϕ_c after which rollover is imminent. The steering threshold is chosen large enough so as to ignore small perturbations. The normalized signals are then each passed through the heuristic notch function h which maps the signals to values in the closed interval $[0, 1]$. The two signals

are then added together and sent through a saturation block such that their sum remains between 0 and 1. Finally, the summed signal is passed through a smoothing filter whose output is α_{M_x}.

As such, the signal α_{M_x} remains near zero, the OFF state, when roll motion and steering action are minimal, and quickly increases to unity, the ON state, when the driver enters a maneuver. Since the signal is a composite of steering angle and roll angle information, α_{M_x} will stay at 1 until the maneuver is complete, after which it will return to the OFF state.

The design of the pitch adaptation parameter is similar, except that instead of roll angle, we consider the pitch angle θ and instead of the steering angle, we use the longitudinal acceleration a_x.

As with α_{M_x}, the signal α_{M_y} remains in the OFF state when pitch motion and forward acceleration are minimal, and quickly reaches the ON state when the vehicle starts pitching, such as while accelerating or breaking. Since the signal is a composite of pitch angle and acceleration signals, α_{M_y} will stay at 1 until the maneuver is complete, after which it will return to the OFF state.

With these parameters in mind, we are ready to incorporate an adaptive process into the control allocation.

Adaptive Allocation

Recall the QP problem formulation (3.36) for the semi-active system:

$$\begin{aligned} \min_{u\in\mathbb{R}^4} \quad & \frac{\gamma}{2}\left\|v - Bu\right\|_{W_v}^2 + \frac{1}{2}\left\|u - u_0\right\|_{W_u}^2 \\ \text{s. t.} \quad & \underline{u}(\dot{z}) \leq u \leq \overline{u}(\dot{z}) \\ & u_0 = F_d(\dot{z}, i_0) \end{aligned}$$

where $\gamma > 0$ is sufficiently large. To make the system adaptive and integrated with local suspension controllers, we redefine two things: the equilibrium control vector u_0 and the weighting matrix W_v.

In the previous section, the vector u_0 was chosen to minimize energy expenditure by the MR dampers by defining its elements by the minimal admissible current. In the case of integrating local suspension controllers, we instead define this vector by the control signals from these local controllers. If, for example, we consider the skyhook control law for the

quarter car model,

$$F_{sky}(\dot{z}_s, \dot{z}) = \begin{cases} C_{sky}\dot{z}_s & \text{if } \dot{z}_s\dot{z} > 0 \\ 0 & \text{if } \dot{z}_s\dot{z} < 0 \end{cases} \tag{3.37}$$

where $\dot{z}_s$ denotes the vertical velocity of the sprung mass at the suspension and $\dot{z}$ is the suspension velocity, we can take $u_0 = [u_{1,eq}, u_{2,eq}, u_{3,eq}, u_{4,eq}]^T$ where

$$u_{i,eq} = F_{sky}(\dot{z}_{s,i}, \dot{z}_i) \tag{3.38}$$

such that the local skyhook suspension control becomes the equilibrium point of the second term of the objective function. It becomes the case, then, that if the first term of the objective function becomes negligible, then the control system reduces to independent skyhook control at each wheel.

Our intuition is clear: we wish to define the weighing matrix W_v for the virtual controls such that it becomes significant in situations where coordinated roll and pitch control is justified, and negligible otherwise. We define $\alpha = [\alpha_{M_x}, \alpha_{M_y}]^T$ and W_v to be

$$W_v(\alpha) = \begin{bmatrix} \alpha_{M_x} & & \\ & \alpha_{M_y} & \\ & & \alpha_{F_z} \end{bmatrix} \tag{3.39}$$

where α_{M_x} and α_{M_y} are the adaptation parameters developed in the previous section. Additionally, we have the parameter α_{F_z} pertaining to the vertical force at the vehicle CG. Since the local suspension controllers are designed to minimize sprung mass motion, then to have this term active at all times would be redundant. Instead, we can define α_{F_z} in the following way:

$$\alpha_{F_z} = \alpha_{M_x} \vee \alpha_{M_y} \tag{3.40}$$

where $\vee$ denotes the maximum element. Thus, whenever roll or pitch control is initiated, vertical CG motion is nonetheless included as a secondary objective. This is useful in situations where a singular vertical excitation (f.e. a large bump under one wheel) occurs during a maneuver.

By the definitions of the adaptation parameters and the weighting matrix W_v, we have that the adaptive QP formulation

$$\begin{aligned} \min_{u \in \mathbb{R}^4} \quad & \frac{\gamma}{2} \|v - Bu\|^2_{W_v(\alpha)} + \frac{1}{2} \|u - u_0\|^2_{W_u} \\ \text{s. t.} \quad & \underline{u}(\dot{z}) \leq u \leq \overline{u}(\dot{z}) \\ & u_0 = F_{sky}(\dot{z}_s, \dot{z}) \end{aligned} \tag{3.41}$$

asserts coordinated control when either the roll or pitch adaptations reach the ON state, and likewise asserts localized suspension control when both are in the OFF state, as desired.

3.2.5 System Stability with the Control Allocator

Assuming no actuator saturations, then the optimal solution to the QP problem is given in closed-form by the equation

$$u = \left(B^T W_v B + \frac{1}{\gamma} W_u \right)^{-1} \left(B^T W_v v - \frac{1}{\gamma} W_u u_0 \right) \tag{3.42}$$

which is a static linear map with inputs v and u_0. Stability of the control allocation is attained if and only if we have

$$\det \left(B^T W_v B + \frac{1}{\gamma} W_u \right) \neq 0 \tag{3.43}$$

which is to say that the mapping $(v, u_0) \mapsto u$ above is well-defined. In this case, the stability of the closed-loop system is determined by the stability of the controllers defining v and u_0. Since the high-level controllers of the previous section were proven to be globally asymptotically stable, then the static control allocation preserves this property, particularly when the control effectiveness matrix B perfectly models the relationship between the virtual controls and the actuator signals.

When actuator saturation occurs, then the combined control system loses global asymptotic stability of the origin, as the system equilibria are perturbed to match the applied disturbances on the vehicle. For example, when the vehicle sustains a cornering maneuver, the lateral acceleration reaches a steady-state value. If the vehicle is equipped with a semi-active system, then the constraints inhibit the actuators from exerting a corrective roll moment in steady-state, which causes the equilibrium roll angle to be nonzero. Such drift phenomena cannot be helped with semi-active actuators, however, the control allocation is nevertheless able to preserve asymptotic stability in cases of high excitation, when saturation is not encountered.

3.3 Simulation Results

The coordinated control system was simulated on a CarSim model of a Chevrolet Equinox. The vehicle entered a fishhook maneuver at a cruising velocity of 100 kph and given no torque input. The fishhook was chosen since the harshness of the maneuver would bring the vehicle close to rollover. As the roll motion is dominant in this maneuver, the controller gains were tuned to emphasize the suspension roll moment. To prevent chattering of the

control signals, the discontinuous sgn functions were replaced by continuous saturation functions in the sliding mode control laws. The semi-active actuators were modeled via the empirical models in (4.1), which will be introduced in the next chapter.

The primary purpose of the simulation study here was to judge the efficacy of the coordinated controller in minimizing the peak roll and pitch angles, as well as vertical vibrations versus ordinary passive damping. It was also of interest was ascertaining whether or not the coordinated control of vehicle roll using suspensions would improve the lateral load transfer, i.e. reduce the peak magnitude of the rollover index

$$\mathrm{RI} = \frac{F_R - F_L}{F_R + F_L} \tag{3.44}$$

where F_R and F_L are the tire forces on the right and left-hand sides of the vehicle, respectively. Peak magnitudes were the prefered metric since in harsh maneuvering with a ground vehicle, the extremes of the dynamics are often what lead to instability, as in rollover.

The optimizer employed in simulation was `qpOASES`, a solver based on an active set method developed for real-time implementation of MPC controllers, but which is also well-suited to online quadratic programming in general [7]. A quantitative comparison between the active, semi-active and passive system simulations is included in Table 4.1.

3.3.1 Active System

The results of the active system simulation can be seen in Figures 3.2, 3.4, 3.8, 3.9, 3.10, and 3.11. The active system greatly improved the angular and vertical responses of the vehicle. The absence of constraints on the actuators enabled the suspensions to drive the angular and vertical dynamics asymptotically to zero. Moreover, the rollover index was effectively controlled by the coodinated suspension system. This indicates that the suspension controller did not deteriorate the vehicle's handling.

3.3.2 Semi-active System

The results of the semi-active system simulation can be seen in Figures 3.3, 3.6, 3.8, 3.9, 3.10, and 3.11. It was supposed that the minimum and maximum admissible currents to the dampers were $i_{min} = 0$ A and $i_{max} = 5$ A. The semi-active suspension system was seen to perform comparably to the active system, except in periods of low excitation in

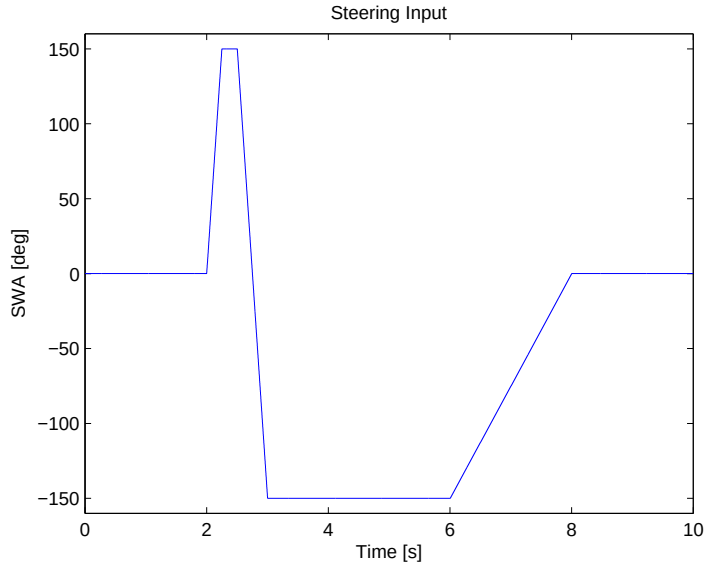

Figure 3.1: Steering input for a fishhook maneuver.

the suspensions. Overall, the optimization-based approach to semi-active control succeeds in attenuating the largest vibrations sustained in the fishhook maneuver. Moreover, like the active system, the semi-active system stabilizes the lateral load transfer (3.44) of the vehicle, effectively preserving the vehicle's handling and adding an element of rollover prevention to the system. As expected, the constraints on the actuators are the limiting factors in the performance of the semi-active system versus the active system.

3.4 Discussion

Overall, the active and semi-active systems performed as expected in simulation. The active system retained the stability properties of the high-level controllers due to the unconstrained nature of the assumed actuators. The drawback of semi-active actuators is obviously the presence of the passivity constraint, which precludes global asymptotic stability of the origin under perturbations of sufficient magnitude. Nevertheless, the control allocation-based approach to semi-active control results in a performance improvement versus passive systems.

Sliding mode controllers were chosen as the preferred high-level controllers in this work, however, there is no particular reason why this should be the case absolutely. Other types

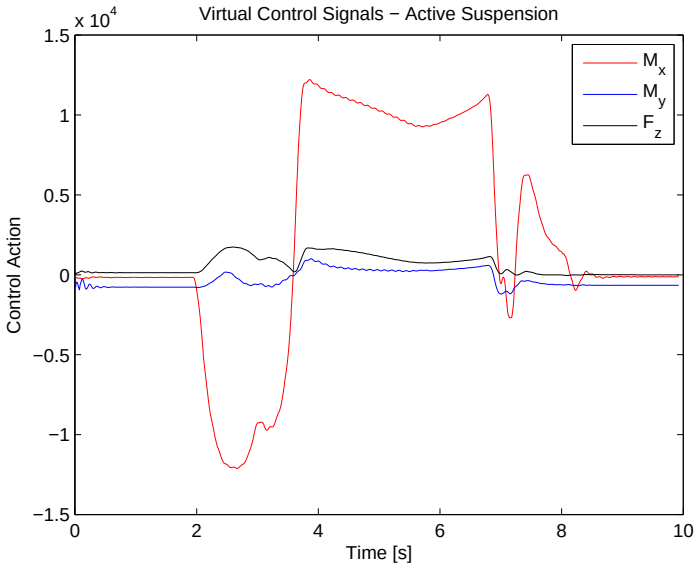

Figure 3.2: Virtual control signals from the active system simulation.

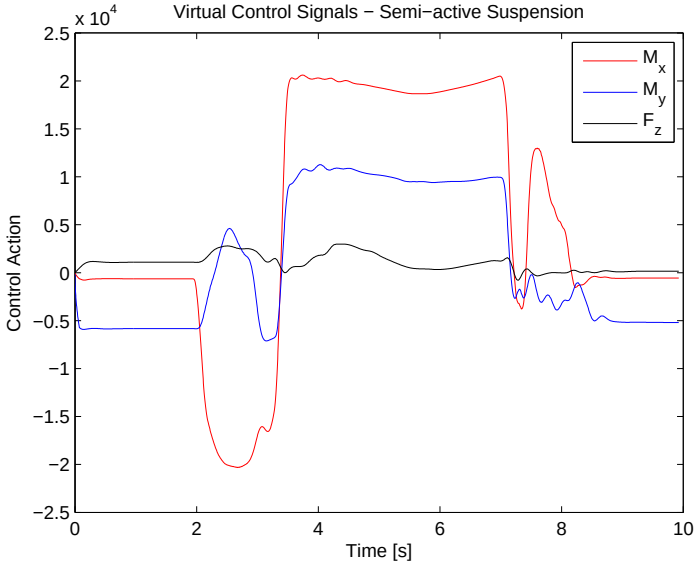

Figure 3.3: Virtual control signals from the semi-active system simulation.

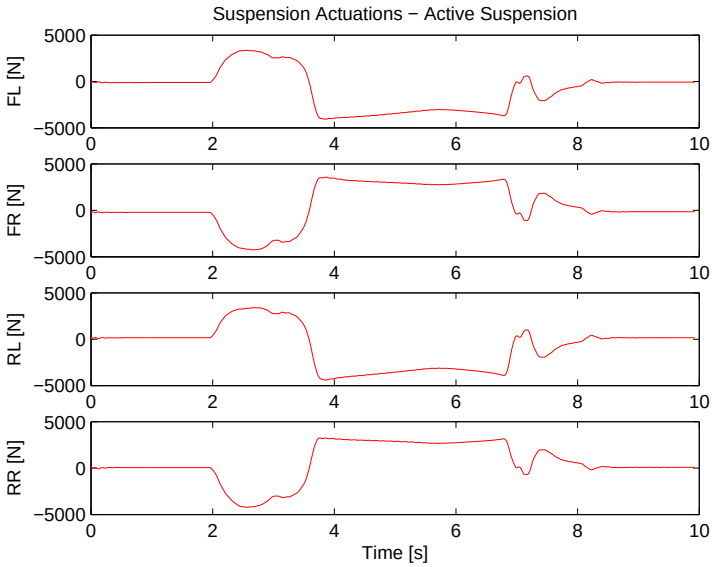

Figure 3.4: Actuator control signals from the active system simulation.

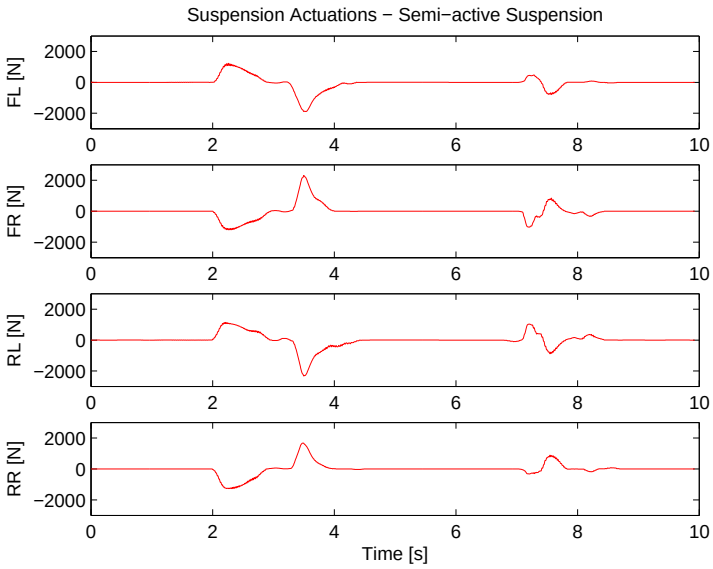

Figure 3.5: Actuator control signals from the semi-active system simulation.

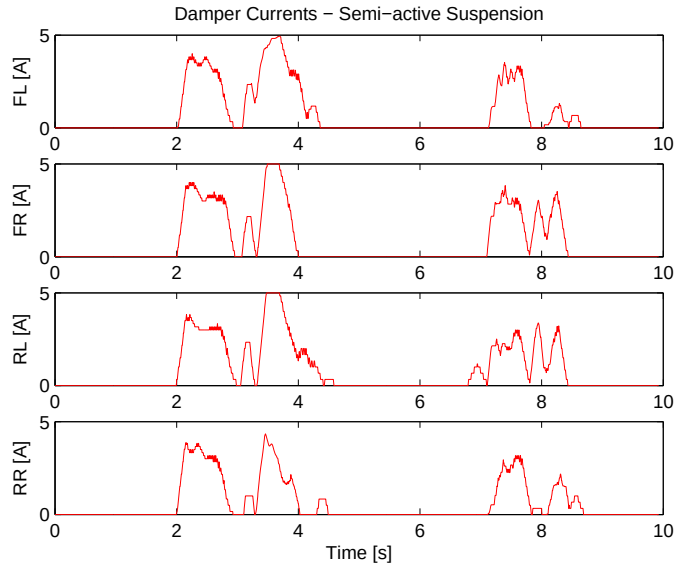

Figure 3.6: Current input signals from the semi-active system simulation.

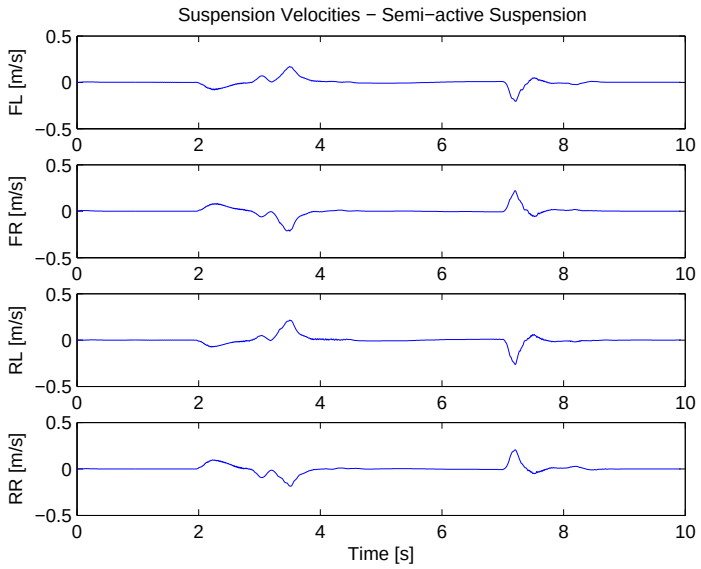

Figure 3.7: Suspension velocities from the semi-active system simulation.

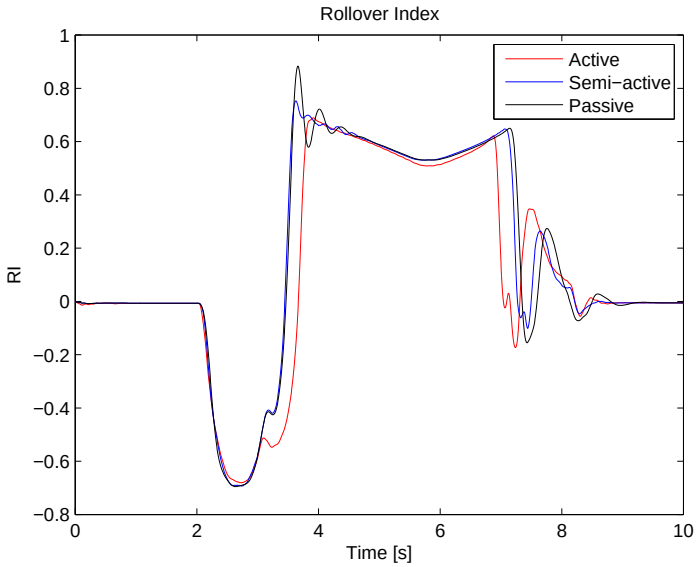

Figure 3.8: Load transfer ratio (rollover index) of the vehicle.

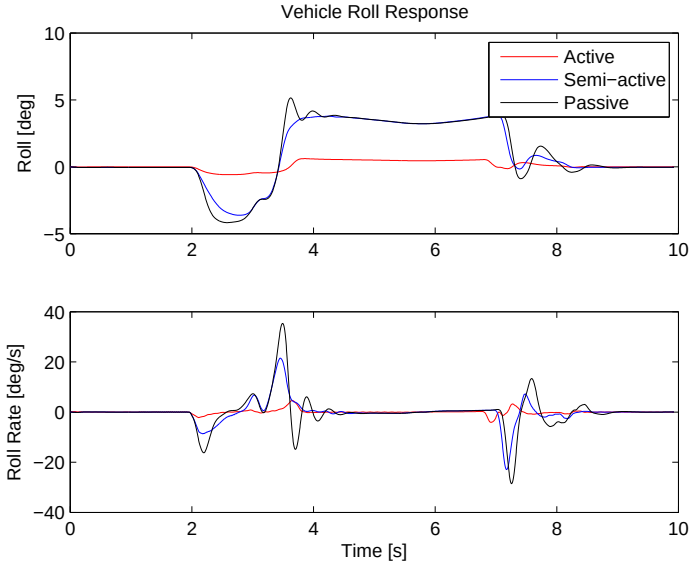

Figure 3.9: Plots of the vehicle's roll response.

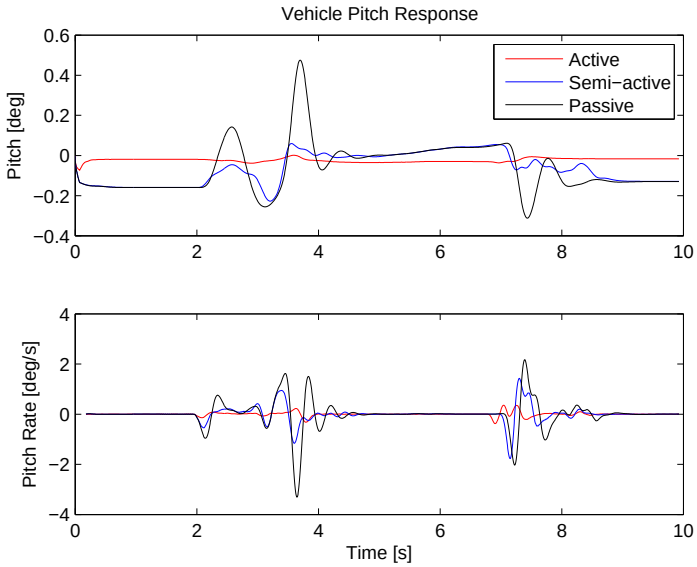

Figure 3.10: Plots of the vehicle's pitch response.

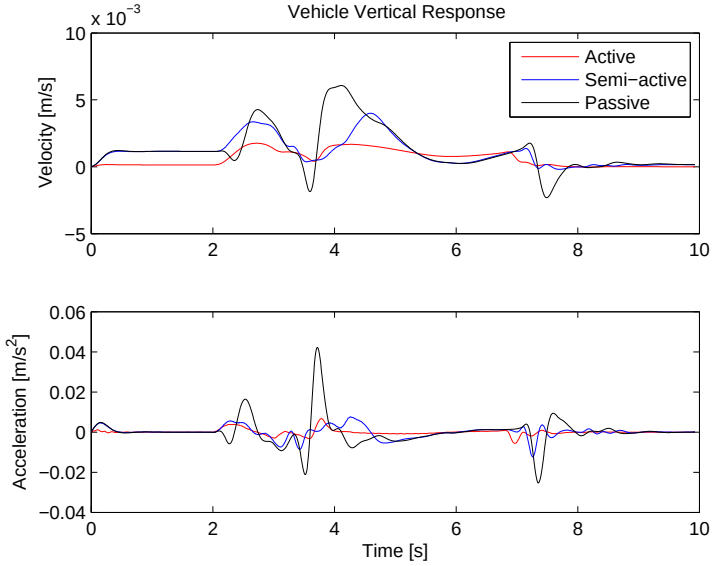

Figure 3.11: Plots of the vehicle's vertical response.

Measure	Units	Passive	Semi-active	Active
Max. Roll Angle	deg	5.14	3.85	0.61
Max. Roll Rate	deg/s	35.3	22.9	4.6
RMS Roll Rate	deg/s	6.40	4.34	0.86
Max. Pitch Angle	deg	0.475	0.227	0.074
Max. Pitch Rate	deg/s	3.31	1.77	0.38
RMS Pitch Rate	deg/s	0.55	0.30	0.07
Max. Vertical Velocity	mm/s	6.1	4.0	1.8
Max. Vertical Accel.	mm/s^2	42.2	12.4	6.7
RMS Vertical Accel.	mm/s^2	7.0	2.8	1.4
Peak Rollover Index	1	0.883	0.753	0.690
Peak Actuation	N	-	2322	4400

Table 3.1: Quantitative measures from simulation.

of controllers with good robustness properties are candidates for use with the control allocation approach to suspension control.

Several assumptions were made in simulation. First, the actuators were considered to be perfect, i.e. that their dynamics were sufficiently fast to justify a static allocation approach, and that they behaved deterministically per the assumed model. The latter is particularly important in the semi-active case, as MR dampers normally exhibit hysteresis and other dynamic loading/unloading behavior. Real actuators with relatively slow dynamics, as might be the case with active suspensions, would require the control allocation to include rate constraints. Secondly, all signals used in control were noiseless. Unfortunately, real measurements are normally corrupted with noise and delays which complicates implementation of control systems. Thus, the simulated system can obviously be viewed as an ideal upper performance limit. Despite these issues, we may conclude that the theoretical features of the controller design are validated in these simulations. □

Chapter 4

Implementation and Experimentation

4.1 Instrumentation and Hardware Design

Traditionally thought of as complex mechanical systems, ground vehicles today are actually better described as complex *mechatronic* systems. As such, any control system developed for modern vehicles requires the integration of mechanical and electrical components as well as computers for proper implementation.

The test platform for the coordinated control system developed in this work was a Cadillac STS maintained by the Mechatronic Vehicle Systems Lab at the University of Waterloo. The suspensions of the STS included stock factory-equipped MR dampers, originally marketed as the MagneRide suspension system developed by BWI Group and which is now standard on many GM vehicles. These dampers, to be used as the actuators in the control system, were driven by PWM servo drivers specially installed in the vehicle for testing of the control algorithm. Furthermore, the STS was outfitted with numerous sensors for real-time data acquisition for control and measurement purposes. These included a six-axis inertial measurement unit (IMU), suspension travel sensors, and laser height sensors attached at the corners of the vehicle body. All sensory data was interfaced with a dSPACE AutoBox, which ran the control algorithm in real-time and produced the PWM signals for the drivers.

In this section, we cover in detail each of the components of the physical implementation of the control system, including models and calibration curves where appropriate.

Figure 4.1: Cadillac STS test platform.

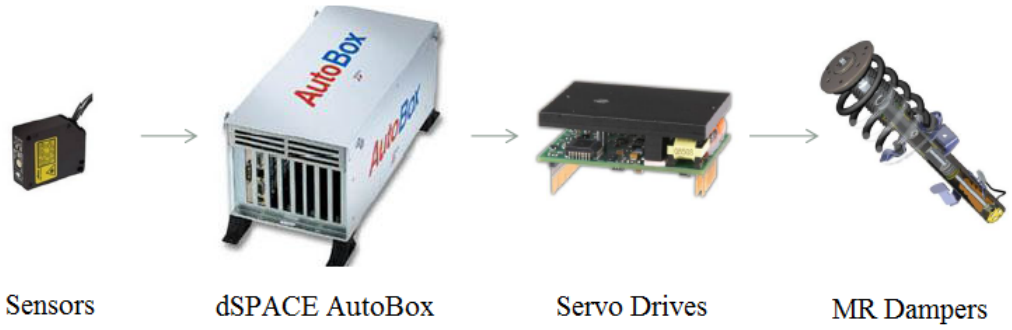

Figure 4.2: Basic overview of the control system instrumentation.

4.1.1 Magnetorheological Dampers

The Cadillac STS used for testing of the coordinated suspension system was outfitted with four factory-equipped MR damper actuators, one at each wheel of the vehicle. As mentioned previously, the MR dampers functioned by inputing a specified electrical current, which by virtue of flowing through a solenoid coil would manipulate the magnetic field within the damper, causing the rheological fluid within to change its stiffness properties accordingly. In order to actually implement the control system, it was necessary to determine the characteristic of the MR dampers, i.e. the relationship between the suspension velocity $\dot{z} = \dot{z}_s - \dot{z}_u$ and current input i to the actuated force from the damper. To this end, statistical models of the dampers were constructed from experimental data. In the following sections, we describe the form of the MR damper characteristics used and present the experimentally determined models.

MR Damper Characteristics

As stated above, an MR damper's force output is typically dependent on the suspension velocity $\dot{z}$ and a given electrical current input i to the damper. The relationship between these quantities and the force output F_d of the damper is nonlinear and, in general, is dynamic, often exhibiting hysteretic behavior. For simplification, we can ignore hysteresis and instead consider a static model of an MR damper described by the functions

$$F_d(\dot{z}, i) = \beta_1 \dot{z} + A(i)S(\dot{z}) \tag{4.1}$$

$$A(i) = \beta_2 i \tag{4.2}$$

$$S(\dot{z}) = \tanh(\beta_3 \dot{z}) \tag{4.3}$$

where $\beta_1, \beta_2, \beta_3 \in \mathbb{R}$ are empirically determined constants, $A(i)$ is called the amplitude function, which depends strictly on current input, and $S(\dot{z})$ is the shape function. In the literature, the amplitude function $A(i)$ is usually taken to be linear, affine or a polynomial of low degree in the current i. In this work, we simply use a linear amplitude function, as that was the general trend observed during experiment. The parameters β_i were estimated by solving a nonlinear least-squares problem on appropriate test data.

For characterizing of the stock MR dampers on the STS, current inputs to the dampers were held constant at values ranging from $i_{min} = 0$ A to $i_{max} = 4.0$ A and the vehicle was made to perform harsh pitching maneuvers such that all four suspensions were excited at varying suspension speeds. The resultant data from the suspension and body travel was then used to estimate the damper force F_d by the equation

$$F_d = m_s \ddot{z}_s + kz \tag{4.4}$$

which is a relationship obtained directly from the quarter-car model. The resultant time responses of the suspension velocity and estimated damper force were lowpass filtered and plotted versus each other in the F_d-$\dot{z}$ plane. From these trajectories, the essentially linear character of the dampers within our operating region was evident, notwithstanding the presence of hysteresis. Two example plots of these phenomena can be seen in Figures 4.3a and 4.3b. Note that the trend of the trajectory of the damper with higher current input has a higher slope than that with the lesser current input. Furthermore, it was observed that the front dampers behaved similarly to each other as did the rear dampers.

In order to identify the regression parameters of (4.1) for each suspension, the planar trajectories resultant from each current trial were combined into a three dimensional point cloud and a multivariable nonlinear regression was performed. These regressions yielded the statistical damper models for the front and rear damper pairs, which can be seen in Figures 4.4a, and 4.4b.

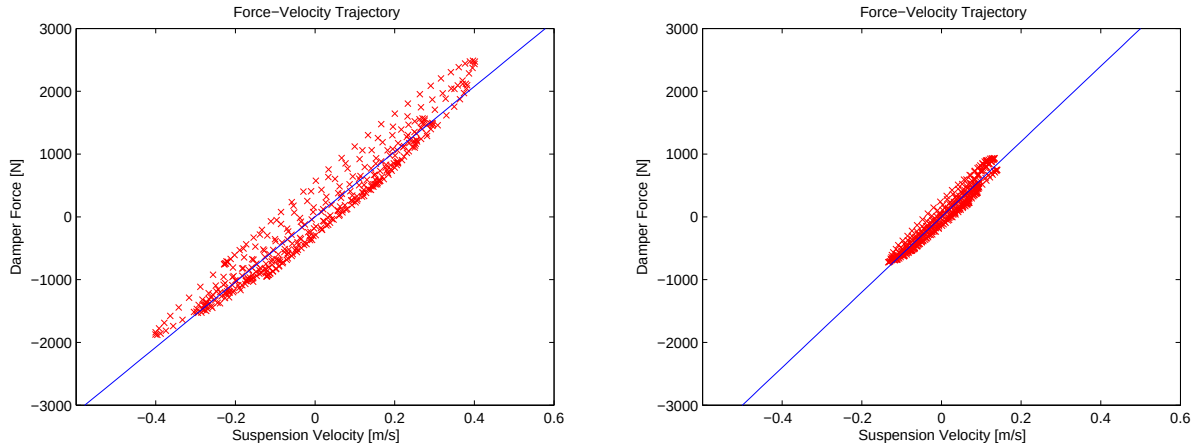

(a) $i = 0$ A (b) $i = 4$ A

Figure 4.3: MR Damper force-velocity trajectory at specified current input.

F_d-$\dot{z}$ to Current Map

For practical implementation of the control system, we need to generate reference current inputs to the MR dampers, given measured suspension velocities $\dot{z}_i$ and desired actuator force outputs u_i. Herein lies the power of applying a regression model such as (4.1). These reference currents can be easily obtained by inverting equation of the empirical model,

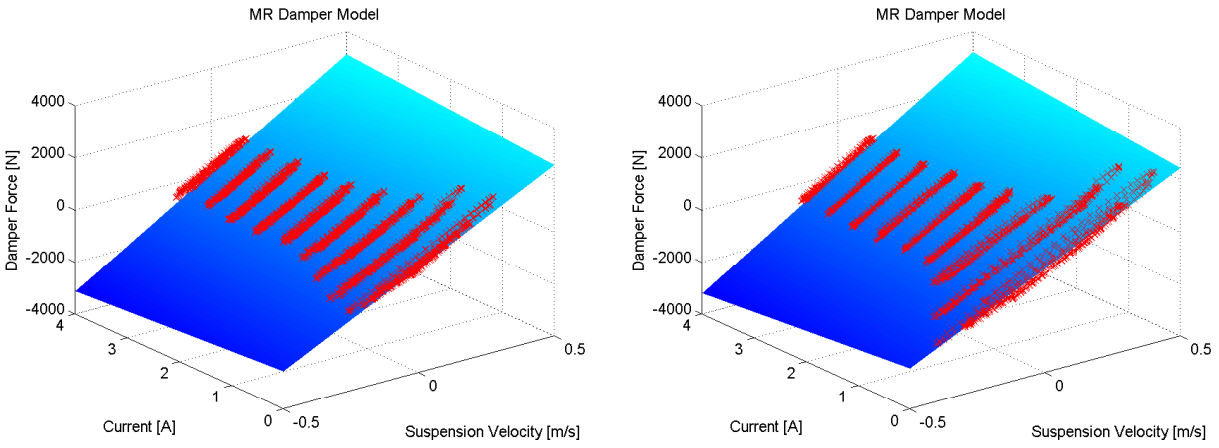

(a) Front (b) Rear

Figure 4.4: MR Damper characteristic surface plots.

solving for i in terms of u_i and $\dot{z}_i$. It is easy to see that the corresponding current inputs i_i are given by the equation

$$i_i = \frac{u_i - \beta_1 \dot{z}_i}{\beta_2 \tanh(\beta_3 \dot{z}_i)}. \tag{4.5}$$

Servo Drivers

Four analog servo drives were installed to provide the necessary current input to the MR dampers for control. The model used was the AZ20A8DDC PWM driver from Advanced Motion Controls. Each of the driver units were powered by a 12 V signal from the car battery via a DC-DC regulator. The stock connectors to the MR dampers were replaced with new ones which were then connected to the servo driver output ports. As mentioned previously, the PWM signals were supplied by the AutoBox.

For calibration, the current output was measured at various duty cycles and a linear regression was done to compute the driver gain. From the calibration curve, it was found that the maximum permissible duty cycle from the control algorithm would be 20 percent (corresponding to a 4.0 A output). Since the resistance across the internal coils of the dampers were determined to be identical, it was assumed that the driver characteristics would be identical. The calibration curve of the servo drivers can be seen in Figure 4.5.

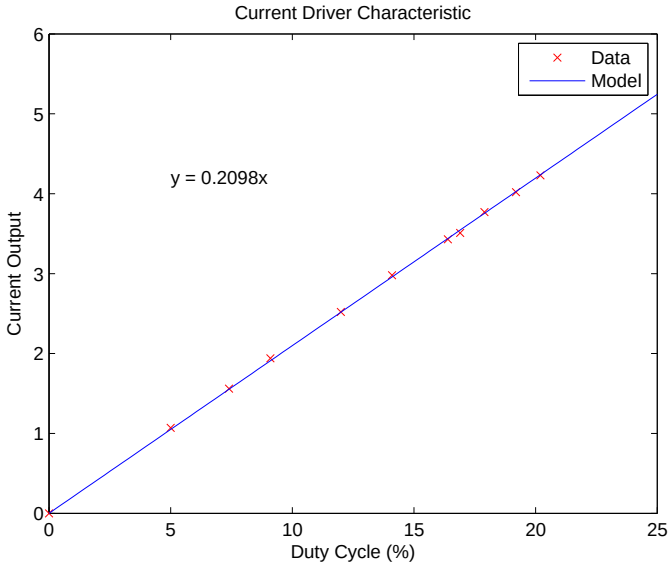

Figure 4.5: Servo driver calibration curve.

4.1.2 Sensors

6-Axis Inertial Measurement Unit (IMU)

The RT2500 6-axis IMU from Oxford Technical Solutions installed on the STS enabled the direct measurement of the linear velocities and accelerations along all principle axes, as well as roll, pitch, and yaw rates. For the purposes of coodinated suspension control, only the lateral and vertical accelerations a_y and a_z, and the three angular velocities were required for feedback, to be used in the high-level controllers. The IMU internally used a combination of measurements from inertial sensors (accelerometers) and GPS with Kalman filtering for processing. The signal outputs from the IMU were interfaced directly with the dSPACE AutoBox via CAN inputs for use in the control algorithm.

Suspension Travel Sensors

Each individual suspension on the STS is equipped with stock linear variable differential transformers (LDVTs) for measuring the suspension travels at each wheel. For use in the coodinated control system, the stock connectors were replaced so that the analog output signals from each sensor were available for feedback. The suspension sensors were powered

by a 5V source from the dSPACE AutoBox. The sensors were calibrated by elevating the car at each wheel and observing the output signal of the sensor for various deflections of the suspension. The sensor output produced was seen to be approximately linear with respect to the suspension travel, as depicted in the following figures.

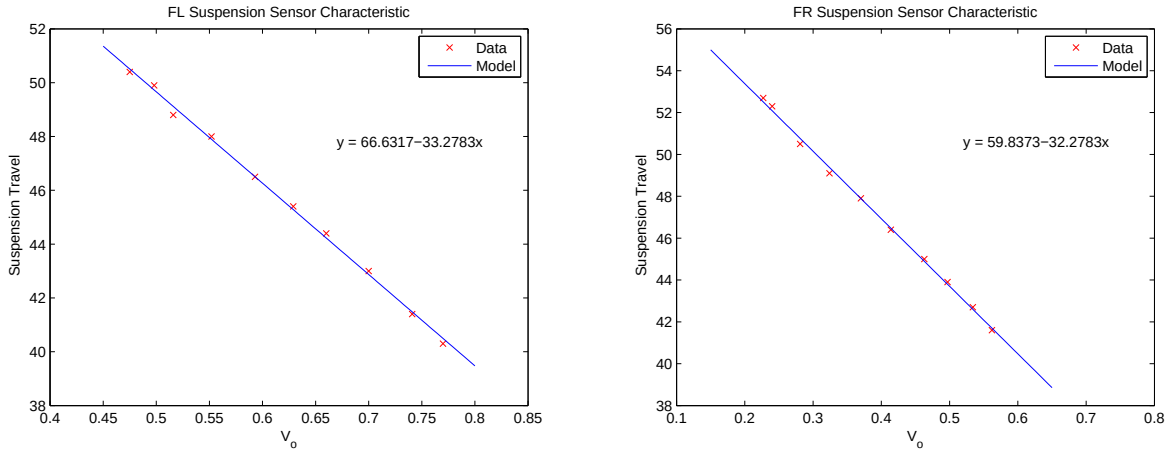

(a) FL

(b) FR

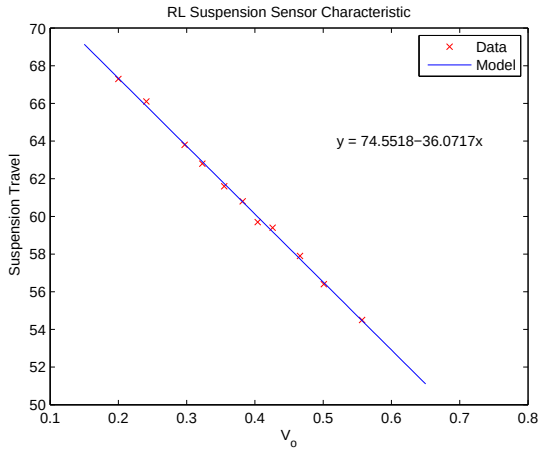

(c) RL

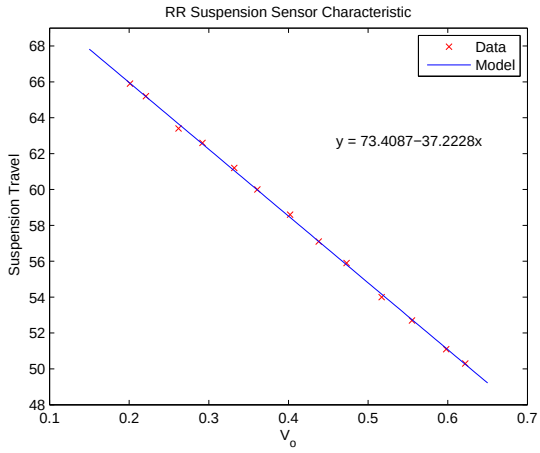

(d) RR

Figure 4.6: Suspension sensor calibration curves.

Body Travel Sensors

Four optical position sensors were mounted to the car body, one at each corner of the sprung mass. These sensors measured the displacement between their mounted position on the body and the ground directly beneath them. Thus, the feedback signals of these sensors provided the measurements of the vertical displacement z_s, i of the body at each corner. The optical sensors were powered directly by the 12V car battery. The analog voltage signals produced by the sensors were seen to be approximately linear within their range of operation, determined by the focal lengths of their internal mirrors. The measurements from these sensors were used to estimate the body roll and pitch angles as well as the vertical position of the sprung mass CG.

4.1.3 Embedded Computing with the dSPACE AutoBox

For real-time implementation of the CSC control algorithm, a dSPACE AutoBox equipped with I/O processor boards and PWM signal generators was installed on the STS. The feedback signals from all installed sensors on the car were directed to the AutoBox for use in the algorithm. In particular, the analog outputs of the suspension and body travel sensors were interfaced with the DS2002 I/O board. The IMU and steering wheel measurements were gathered from the DS4302 CAN interface board. Single-phase PWM signals to be generated by the control algorithm were delivered to the current drivers from the output pins on the DS4002 board. The 5V signal powering the suspension sensors was also supplied via the DS4002.

The dSPACE AutoBox provided the computational muscle required to implement the coordinated control algorithm in real-time, i.e. to continuously solve QP problems for the optimal control distribution. Discussion of the software design continues in the next section.

4.2 Software Design

As is standard on all modern vehicles equipped with ESC and other digital control algorithms, on-board software is prohibited to be written by hand, per industry safety regulations. As such, the control algorithms were coded in Simulink and then converted automatically into ANSI C code and compiled using a special compiler by dSPACE specifically designed for generating code for the AutoBox.

The software architecture of the control system consisted of four parts: the Input Processing block, for reading and transforming sensor data, the High-Level Controllers, for generating the virtual control signals, the Control Allocator, for optimal distribution of the actuator controls, and the Output Processing block, for generating reference currents and duty cycles for the servo drivers. In this section, we describe each of these four modules in detail.

4.2.1 Input Processing and Estimation

The Input Processing block took as input the vector `Input` of all measured signals from the sensors deployed on the vehicle. The module had three functions: to convert all measured signals into the required units, to estimate all other required quantities from the measured data, and to compute the adaptation parameters α.

The inputs to the dSPACE AutoBox, being analog voltage readings from the suspension and body travel sensors, needed to be converted into appropriate units for use with the control algorithm. The analog signals from the DS2002 board were read through a specialized DS2002 32-channel Multiplexer ADC function. Then, using the regression models of the sensors presented in the previous sections, the analog inputs were transformed into the necessary kinematic data. Data from the IMU interfaced with the DS4302 CAN bus was read through RTI CAN Receive Message functions. As these signals were digital, conversions of these measurements into appropriate units was done using simple gain functions.

From the sensory data, other quantities necessary for control of the vehicle could be computed or estimated. Signal noise was removed by using discrete first-order filters (weighted moving average filters). In particular, the suspension and body travel data were passed through triangular smoothing filters to remove noise and were then sent through discrete derivative blocks to obtain their velocities. The roll and pitch angles as well as the displacement of the sprung mass CG were estimated from the measured body travel data.

Computation of the adaptation parameters for roll and pitch control was performed in the way specified in the previous chapter. All measured and estimated quantities were passed as output from the block in a single vector `InputP` for use in other modules. The vector of adaptivity parameters `Alpha` was also output for use in the control allocation block.

4.2.2 High-Level Controllers

The High-Level Controller module took as input the vector of processed inputs and estimated quantities `InputP`, and output the vector of virtual control signals `v`. This vector contained the two generalized moments M_x and M_y, the generalized CG force F_z, and the four localized suspension controls u_0. The roll moment M_x was defined by the sliding mode control law (3.4) and the pitch moment M_y and vertical CG force F_z were defined by the control law (3.16). The localized suspension controls were defined by the hybrid skyhook-groundhook semi-active control law. The vector `v` of these virtual control signals was output to the control allocation module for distribution.

4.2.3 Control Allocator

The Control Allocator module took as input the vector of processed inputs `InputP`, the vector of virtual control signals `v`, the vector of adaptation parameters `Alpha`, and a vector of boolean values `Fault`. The purpose of the control allocator was to solve the constrained QP problem (3.41) for the actuator forces u. This was accomplished in two parts: the computation of all necessary quantities for the optimization problem, and the real-time solution of the quadratic program.

The quantities necessary to define the optimization problem included the weighting matrices W_v and W_u, and the control effectiveness matrix B in order to define the objective function, as well as the vector of upper bounds $\overline{u}$ and lower bounds $\underline{u}$ for the actuator controls, defining the set of feasible values $\mathcal{U}$. In particular, the weighting matrix W_v was computed dynamically using the adaptivity parameters in the vector `Alpha`, and the actuator bounds were computed using the statistical MR damper characteristics. The `Fault` array, consisting of four boolean values encoded information on the fault state of the actuators. If for each `true` value in `Fault`, the corresponding actuator was removed from the optimization process. This was done by simply setting the corresponding columns of B and elements of u_0 to zero.

The solution of the quadratic programming problem was performed using the `QCAT` toolbox developed by Härkegård [9]. The specific function used was a modified version of `wls_alloc`, which applies an active set algorithm for solution of control allocation problems defined by quadratic programs. Modifications were made to the code so that it could compile on the dSPACE AutoBox. In particular, the reliance on dynamically-sized arrays and logical indexing were removed. The output of the optimization process was the vector `u` containing the four actuator controls, and the quantity `qpIter` which counted the number of iterations required by the solver to find the optimal solution.

4.2.4 Output Processing

The Output Processing module, the final module of the control code, took as input the vector of processed inputs `InputP` and the vector `u` of actuator controls computed by the control allocator. The purpose of the output processing block was to transform the output from the control allocator into reference currents to be transmitted to the MR dampers. This was accomplished by using the inverse mapping (4.5) using the actuator controls u_i and the suspension velocities $\dot{z}_i$. Once computed, these electrical current values were transformed into the equivalent duty cycle for the PWM signals sent to the servo drivers using the linear regression curve derived previously. To reduce chattering, current outputs were deadbanded while the estimated suspension velocity remained within a specified tolerance about zero.

4.3 Experimental Results

The coordinated control system was tested in real-time on the Cadillac STS for validation of the algorithm. As the primary signals of interest were roll and pitch responses, two experiments were carried out to excite each motion: double lane-changes were performed to excite body roll, and stopping tests (heavy braking from 70 kph) were performed to excite pitch. All tests were conducted on smooth road on the driving track at the Region of Waterloo Emergency Services Training Area.

The online solver used for the control allocation was `QCAT`, rather than `qpOASES` as in simulation. This decision arose from an incompatibility of `qpOASES` with the AutoBox. It was nevertheless determined that both software packages yielded the same optimal solutions, with `QCAT` requiring on average a couple more iterations than `qpOASES`.

In interpreting the results of the following experiments, statistical significance tests were used to make inferences about the coordinated control system from the data collected. In this work, we consider two levels of confidence: $\alpha = 0.05$, which corresponds to "good" confidence in the result, and $\alpha = 0.1$ for "low" confidence.

4.3.1 Double Lane-Changes

The double lane-change test involved accelerating the car to 60 kph and executing two sequential lane-changes. The resulting lateral acceleration from the maneuver excited the roll mode of the car. This experiment gave a comparison between the coordinated

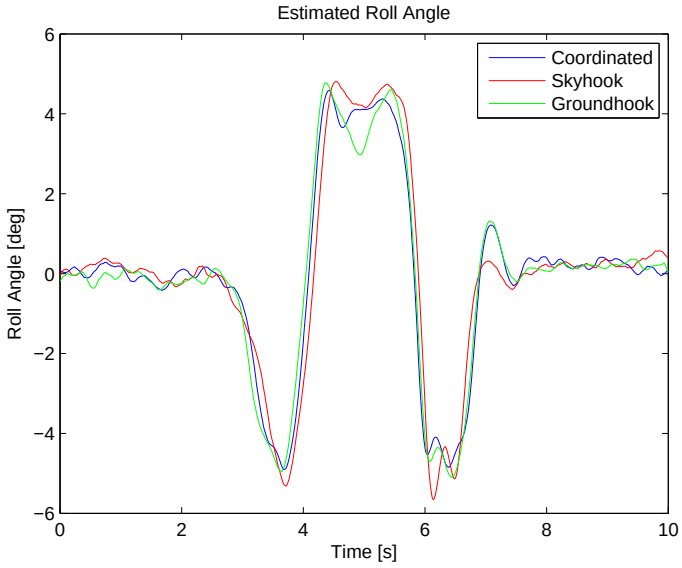

Figure 4.7: Roll response from Trial 1 of the double lane-change test.

system, pure skyhook, and pure groundhook controllers. In accordance with the situational adaptivity of the controller, the α_{M_x} parameter quickly reached the ON state during the lane-changes, engaging coordinated roll control, and the α_{M_y} parameter reached the ON state during the acceleration and braking before and after the maneuver.

The maximum roll angles of all trials were recorded and the sample mean for each controller type was computed. Assuming that errors about the "true" mean of these statistics were normally distributed and with the same variance across all controller types, two-sample t-tests were performed to ascertain the statistical significance between the difference of the means of the sample statistics. The null hypotheses tested were: (1) "there is no difference in roll angle attained between skyhook and coordinated control", and (2) "there is no difference in roll angle attained between groundhook and coordinated control". Testing suggested that the coordinated roll control gave an improvement on pure groundhook control with good confidence ($p < 0.05$) and an improvement on pure skyhook with low confidence ($p < 0.1$). The same proceedure was done with peak measured roll rates, however, the differences in roll rate among the controllers tested were not deemed to be statistically significant ($p > 0.1$).

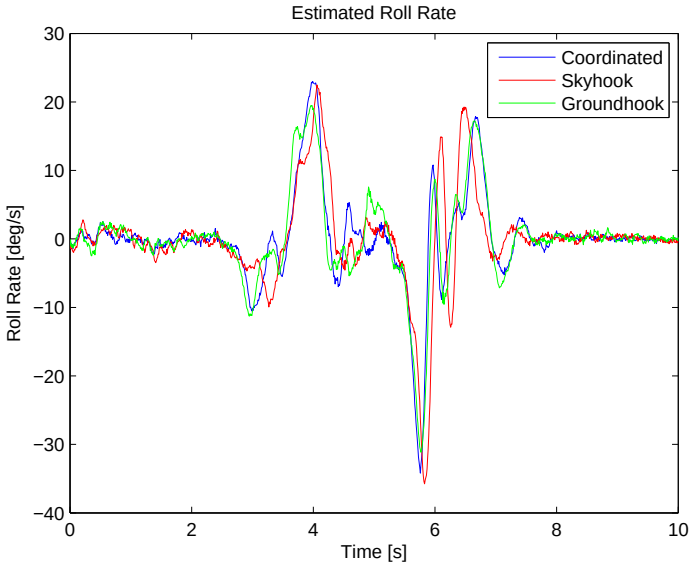

Figure 4.8: Roll rate response from Trial 1 of the double lane-change test.

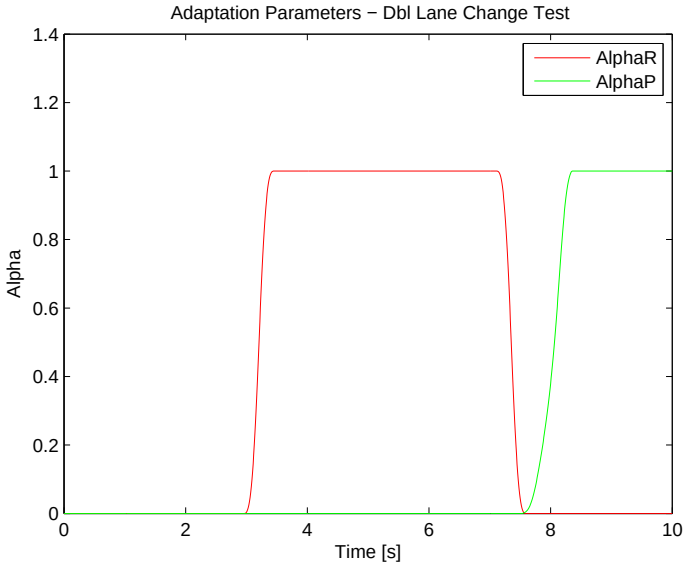

Figure 4.9: Adaptivity parameters in a double lane-change. The pitch parameter activates at the end when breaking is initiated.

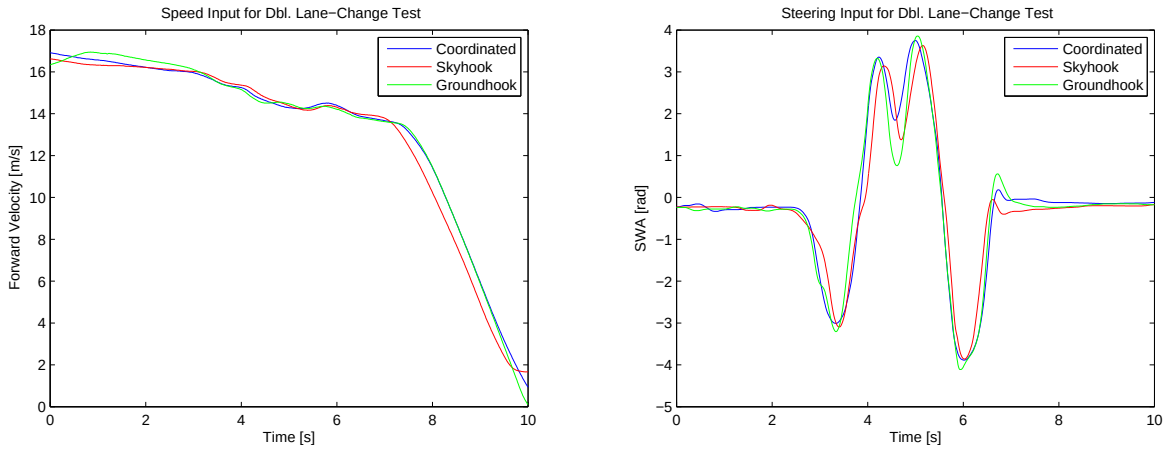

(a) RL

(b) RR

Figure 4.10: Speed and steering inputs in Trial 1 of the double lane-change test.

4.3.2 Stopping Tests

The stopping tests involved accelerating the car to 65 kph and proceeding to brake with as much pedal pressure as possible. As with the double lane-changes, this experiment gave a comparison between the proposed controller, pure skyhook, and pure groundhook implementations. In accordance with the adaptivity feature, the α_{M_y} parameter reached the ON state during the acceleration and braking phases of the maneuver.

As with the double lane-change experiment, the maximum pitch angles of all trials were recorded and the sample mean for each controller type was computed. Assuming that errors about the "true" mean of these statistics were normally distributed and with the same variance across all controller types, two-sample t-tests were performed to ascertain the statistical significance between the difference of the means of the sample statistics. The null hypotheses tested were: (1) "there is no difference in pitch angle attained between skyhook and coordinated control", and (2) "there is no difference in pitch angle attained between groundhook and coordinated control". Testing suggested that the coordinated pitch control gave an improvement on pure groundhook control with low confidence ($p < 0.1$) but did not give a statistically signficant result versus skyhook control ($p > 0.1$). The same proceedure was done with peak measured pitch rates, however, the differences in pitch rate among the controllers tested were also not deemed to be statistically significant ($p > 0.1$).

Measure	Units	Skyhook	Groundhook	Coordinated
Max. Roll Angle	deg	5.654	5.103	4.907
RMS Roll Angle	deg	2.420	2.343	2.327
Max. Roll Rate	deg/s	35.76	31.16	34.20
RMS Roll Rate	deg/s	7.125	6.791	6.764

Table 4.1: Quantitative measures from Trial 1 of the double lane-change test.

Measure	Units	Skyhook	Groundhook	Coordinated
Max. Roll Angle	deg	5.232	5.068	4.858
RMS Roll Angle	deg	2.368	2.183	2.157
Max. Roll Rate	deg/s	24.72	25.50	28.25
RMS Roll Rate	deg/s	6.528	6.032	6.536

Table 4.2: Quantitative measures from Trial 2 of the double lane-change test.

Measure	Units	Skyhook	Groundhook	Coordinated
Max. Pitch Angle	deg	2.290	2.610	2.140
RMS Pitch Angle	deg	1.387	1.484	1.344
Max. Pitch Rate	deg/s	13.77	10.80	11.06
RMS Pitch Rate	deg/s	1.938	2.193	1.937

Table 4.3: Quantitative measures from Trial 1 of the stopping test.

Measure	Units	Skyhook	Groundhook	Coordinated
Max. Pitch Angle	deg	1.936	2.474	1.810
RMS Pitch Angle	deg	1.326	1.389	1.283
Max. Pitch Rate	deg/s	9.530	12.57	12.83
RMS Pitch Rate	deg/s	3.102	2.555	2.882

Table 4.4: Quantitative measures from Trial 2 of the stopping test.

Measure	Units	$\overline{x}_{sky}$	σ^2_{sky}	$\overline{x}_{gnd}$	σ^2_{gnd}	$\overline{x}_{CSC}$	σ^2_{CSC}
Max. Roll Angle	deg	5.443	$8.9 \cdot 10^{-2}$	5.085	$6.4 \cdot 10^{-4}$	4.883	$1.2 \cdot 10^{-3}$
Max. Pitch Angle	deg	2.113	$6.3 \cdot 10^{-2}$	2.542	$9.4 \cdot 10^{-3}$	1.975	$5.2 \cdot 10^{-2}$
Max. Roll Rate	deg/s	30.24	60.96	28.33	16.02	31.22	17.70
Max. Pitch Rate	deg/s	11.65	8.99	11.68	1.566	11.94	1.566

Table 4.5: Sample means and variances from test data.

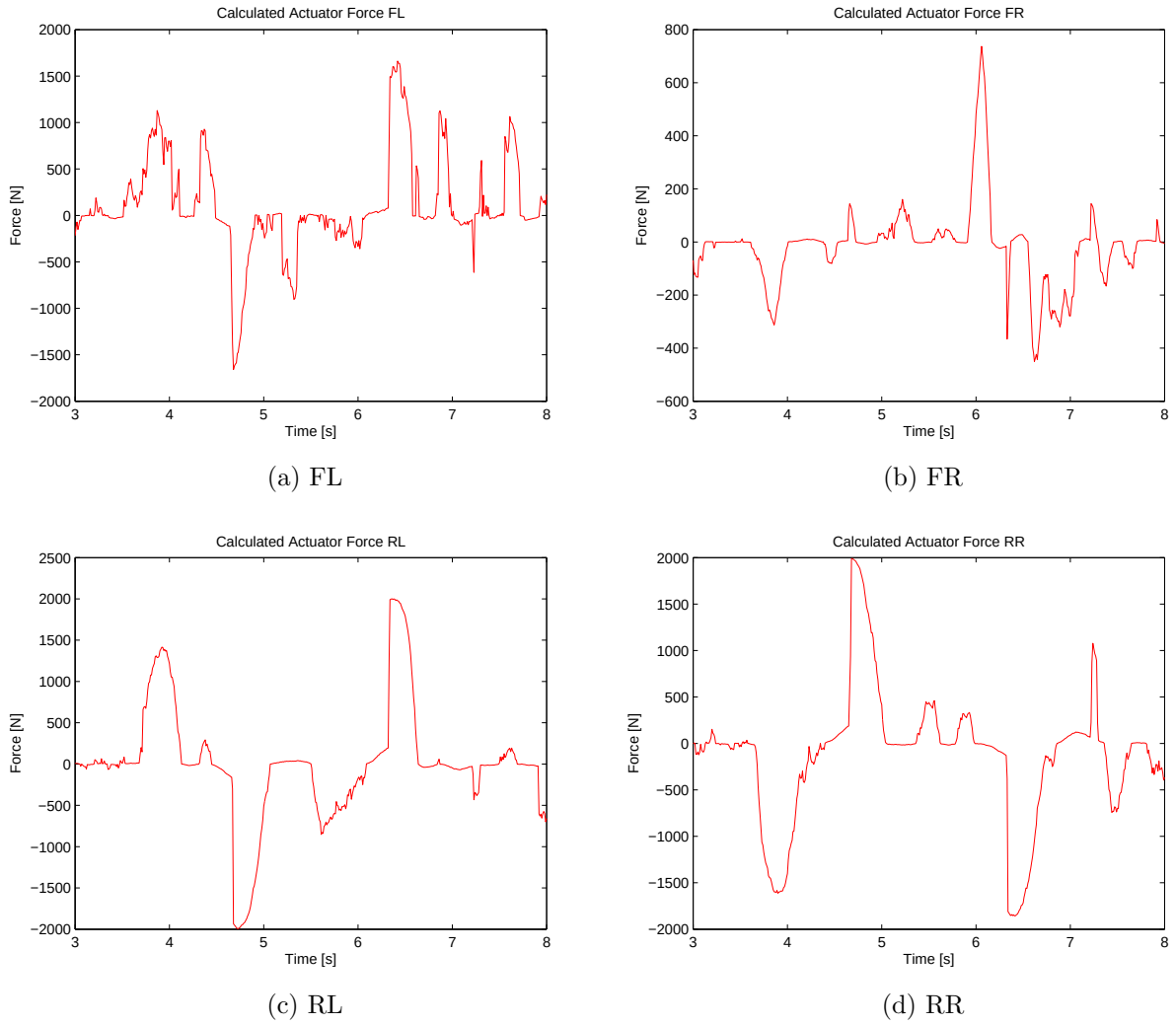

(a) FL

(b) FR

(c) RL

(d) RR

Figure 4.11: Calculated force outputs from the double lane-changes.

4.4 Discussion

Overall, the coordinated controller succeeded in improving the roll and pitch responses versus the standard semi-active control methods, as can be seen from the raw data of tables 4.1 through 4.4. Additionally, we have some grounds for claiming that the coordinated system is more suited to roll and pitch control than standard single-corner implementations via statistical analysis. This is consistent with the explicit nature of the roll and pitch

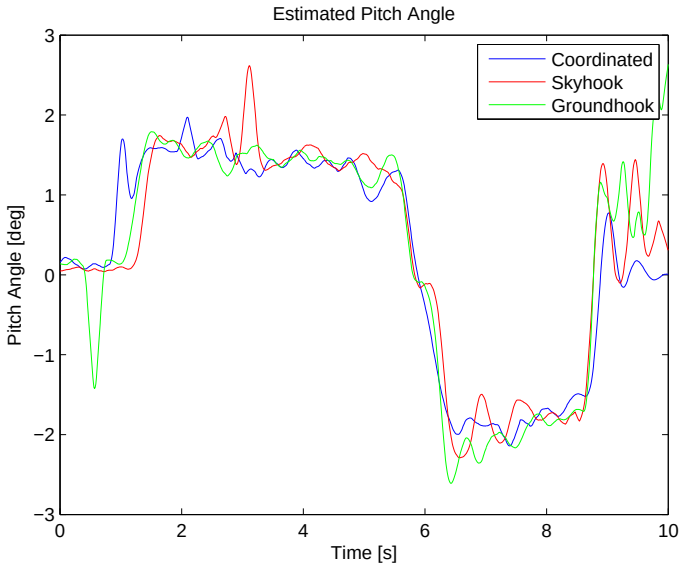

Figure 4.12: Pitch response from Trial 1 of the stopping test.

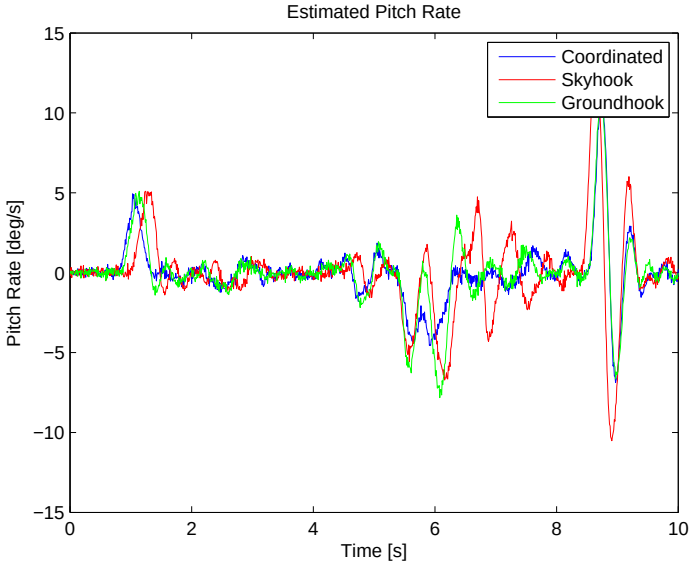

Figure 4.13: Pitch rate response from Trial 1 of the stopping test.

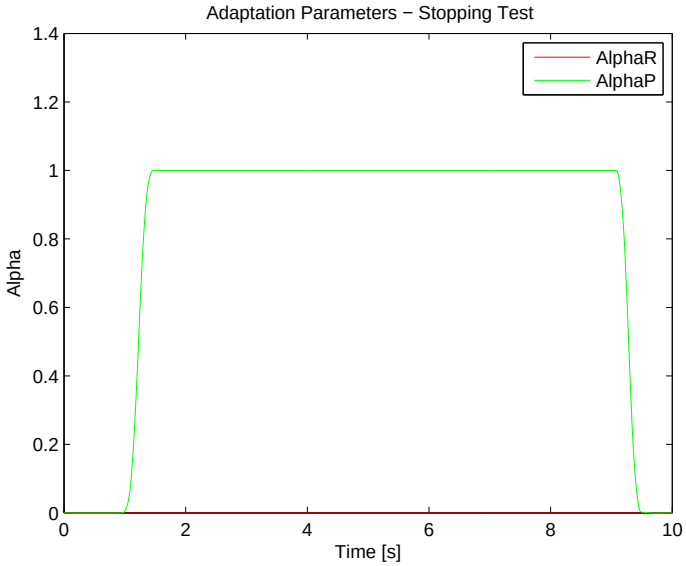

Figure 4.14: Adaptivity parameters in a stopping test. The pitch parameter is active throughout the accelerating and breaking phases of the maneuver.

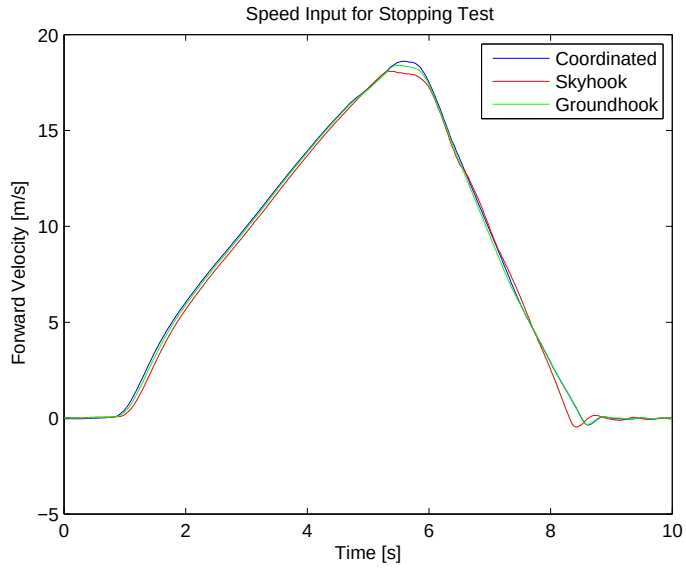

Figure 4.15: Speed inputs in Trial 1 of the stopping test.

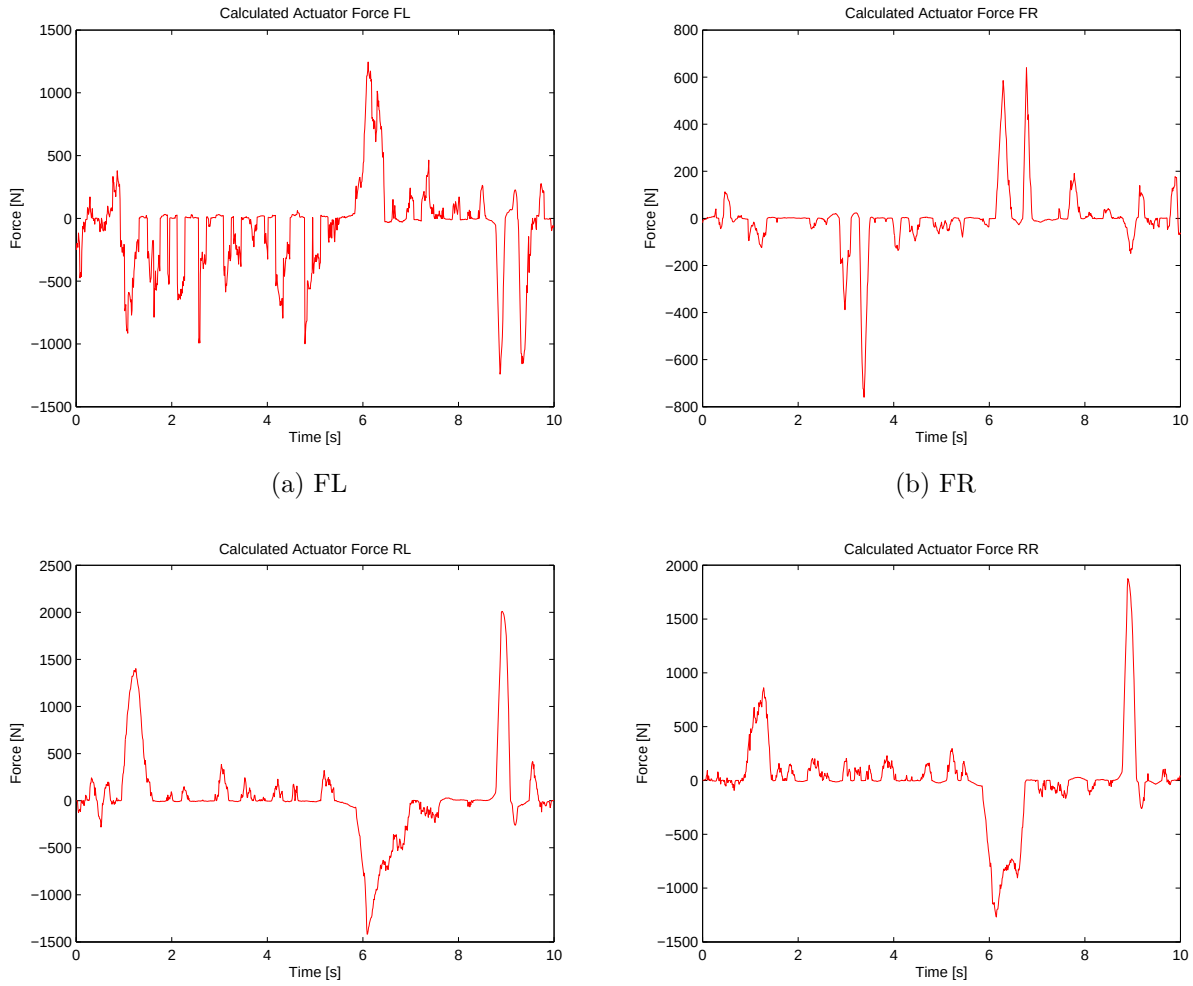

(a) FL

(b) FR

(c) RL

(d) RR

Figure 4.16: Calculated force outputs from the stopping tests.

control in the optimization procedure, versus the supposed indirect control of these degrees of freedom via single-corner control.

As a handling-based controller, the groundhook method performed better than skyhook in the double lane-change test in terms of both roll angle and roll rate. The coordinated controller matched groundhook in this case for the most part, with slight improvement in roll angle control. Notably, the peak roll rate of the vehicle with the coodinated controller

Measure	Controller 1	Controller 2	t-score	p-value	Reject $\mathcal{H}_0$?
Max. Roll Angle	Coordinated	Skyhook	2.6405	0.0593	Yes*
		Groundhook	6.7195	0.0214	Yes
Max. Pitch Angle	Coordinated	Skyhook	0.5698	0.6263	No
		Groundhook	0.5698	0.0865	Yes*
Max. Roll Rate	Coordinated	Skyhook	0.1569	0.5318	No
		Groundhook	0.7050	0.5538	No
Max. Pitch Rate	Coordinated	Skyhook	0.1284	0.9096	No
		Groundhook	0.2077	0.8547	No

Table 4.6: Student's t-test results and p-values. An asterisk denotes meeting the low confidence threshold $\alpha = 0.1$.

is more comparable to the skyhook response, however the RMS of the roll rate with the coordinated controller is more similar to the groundhook response. In terms of maximum roll angle, the t-tests showed that the coordinated system faired better than groundhook control with good confidence ($p < 0.05$). Improvement versus skyhook control was seen as well, however with a lower confidence.

According to the data, the skyhook controller performed better than the groundhook controller in the stopping test. This is probably because the pitch motion in the stopping test is due more to pure sprung mass vibration rather than wheel motion or load transfer. In pitch control, the coodinated strategy matched the skyhook response with a slight improvement in the angular and rate responses. Moreover, the maximum pitch rate of the vehicle with the coodinated controller gave an improvement on the skyhook control, matching more closely the groundhook response, though still slightly higher. In terms of maximum pitch angle, the t-tests showed that the coordinated system faired better than groundhook control with low confidence ($p < 0.1$), but not versus skyhook control.

From the data, we see that the coodinated controller achieves responses comparable to both skyhook and groundhook depending on the situation. As such, the coordinated suspension control system can be thought of as a form of hybrid control. Moreover, the data appears to suggest that the explicit inclusion of roll and pitch control in the controller design allows for improvement of these responses, as hypothesized in [4].

As we have seen in the previous section, the control system designed in this work succeeded in improving the pitch and roll responses of the vehicle system tested versus the purely passive case. In the current implementation, the results do not quite scale to those expected from simulation. This can be for a number of reasons, among them the

loss of the "perfect actuator" assumption, the presence of noises in the signals and the consequent effects of delays from filtering. All of these issues, conspicuously absent from the simulations, were present in the real-world system and hence degraded performance.

Simulations assumed that the MR dampers behaved precisely like the statistical models (4.1), and that the suspension velocities were perfectly known. The damper forces calculated in simulation were therefore at best approximate, as it was observed that the real MR dampers exhibited hysteresis. Signal noise, particularly in the suspension travel sensors, was prevalent. As the suspension travels needed to be differentiated to obtain their velocities, the signals needed to be strongly prefiltered. This resulted in a time delay of a few hundredths of a second, which in dynamic situations is rather significant, as vibrations in the suspensions can occur at very high frequencies. No such delay was considered in simulation since filtering was unnecessary.

It must also be remembered that vehicle testing can be somewhat subjective. In testing, several practice runs were performed beforehand so that the driver could perform the test maneuvers with relative consistency. This was particularly important for the double lane-changes, being the more technical of the two chosen tests. Since the vehicle tests were performed by a human, slight discrepancies in the steering (double lane-changes) or applied break pressure (stopping tests) between test runs constitute a probable source of systematic error. From Figures 4.10 and 4.15, we can see that the test runs performed are relatively consistent. Additionally, environmental factors are a potential source of random error in the experiment. Though as the tests were performed on a sunny day with low wind and on a dry track, this error could be considered negligible. These sources of error could be alleviated by substituting the human driver by a computer, and by testing in a large, indoor facility.

The t-tests were performed in order to make more educated inferences from the test data given the presence of uncertainties in the system during testing. Overall, the statistical analysis suggested that the coordinated system controlled roll and pitch angles better than single-corner controllers, but with lower confidence than would be desired in some cases. Of note is that only two trials were performed for each maneuver. Repeating the experiment with more trials could potentially bring the p-values of interest down to the desired level. On the other hand, the low p-value in the coordinated vs. groundhook roll control comparision might be attributable to the low sample variance in the groundhook case. Performing more trials might increase the sample variance, thus increase the p-value into the low confidence range.

Finally, another issue was the test vehicle itself, in particular the stock MR dampers. In characterizing the dampers in 4.1.1, it was observed that the change in damping between

the 0 A to 4 A inputs barely exceeded 15 percent, which is miniscule. To avoid frying the dampers in testing, the current inputs were limited to 4 A. It is possible that raising this limit in the algorithm can improve the range of the dampers, though at a risk. In general, semi-active control can achieve a much higher standard if the range of damping is increased. Furthermore, as the Cadillac STS used was a pre-production model from 2006, the MR dampers used in experiment were likely not state-of-the-art, thus it is plausible that improved performance using the coordinated control system can be achieved with a simple upgrade of the semi-active actuators, let alone the possibility of testing the algorithm with active suspensions like the Bose system. □

Chapter 5

Conclusions and Future Work

5.1 Conclusions

Revisiting the central question of this thesis, whether we can generalize suspension control (particularly semi-active control) to encompass all vertical vehicle dynamics in a coordinated way, which would be integrable with modern ESC systems, we can affirmatively say "yes". The coordinated suspension control system, or CSC, does exactly that through the application of control allocation techniques. Such a formulation has the advantage of explicitly designing the controller to improve roll and pitch responses, which is often not considered at all in suspension controllers, semi-active control laws in particular.

We have seen that the coordinated system improves the vehicle response compared to passive suspensions. As well, we have seen that the given implementation is comparable to other handling-oriented semi-active control strategies designed for a single-corner, like groundhook control. The promise shown by this type of coordinated system is especially evident in the wake of the development of active suspensions, but may also find utility when formulated with conventional semi-active adaptive actuators. Further development is required to optimize the CSC system, however, before it can be definitively stated that it is superior to single-corner implementations.

5.2 Recommendations for Future Work

We conclude this work with some recommendations for future research and development based on the experiences acquired during the course of this project.

Refining of Actuator Models

In section 4.1.1, the MR dampers on the Cadillac STS were characterized by fitting a static statistical model to experimental data. Owing to the approximate nature of these characteristics because of modeling errors and noisy data, some performance degradation was to be expected. Therefore, more accurate models of the equipped dampers should improve performance. Much exists already in the literature on the modeling of the dynamics of MR dampers, many being variations on the well-known Bouc-Wen model. Ideally, one or two of the STS dampers should be removed from the car and tested in a lab with a force generator to map out their characteristics in the most accurate way possible. Afterwards, the data can be fit to a possibly more complicated, dynamic model and the problem of integrating this new model with the control allocation can then be explored.

Improved Filtering and Estimation

Signal noise is an ever present annoyance in engineering systems and a primary source of performance degradation, and this system is no exception. Sources of noises in the control system included both mechanical and electrical vibrations. In particular, the suspension travel sensors were quite noisy, and had to be heavily filtered for use in the algorithm. Research into sensor technology and filtering techniques could greatly impact performance gains. In order to sidestep the task of differentiating the suspension sensor signals, it might be more appropriate to apply a rate linear encoder for direct measurement of the suspension velocities, as the relative *displacement* of the suspensions themselves are not useful, whereas the velocity is key to proper implementation of the algorithm. The primary drawback to this is an increased cost of implementation.

In testing of the control system, multiple sensors were deployed for direct measurement of the required signals. For commercialization, the number of these sensors should be minimized. In particular, the body travel sensors are prime candidates for replacement via estimation algorithms. Moreover, performance might be improved by use of parameter estimation modules to further account for parametric uncertainties.

Research into Active Suspension Systems

Simulation in section 3.3.1 suggests that the coordinated control of the suspensions can deliver complete regulation of the vertical dynamics to zero state, assuming a perfect set of actuators. It remains to develop a commercially available active suspension which can

deliver the power required for this task with the necessary bandwidth. When such an actuator can be fitted to a test vehicle, the active form of the control algorithm explored in this thesis can be tested. In the case that the active actuators do not possess the required bandwidth, it might also be worthwhile to explore ideas of dynamic control allocation, which can incorporate the actuator dynamics into the control allocator design.

Integration and Testing with ESC Systems

As seen in the literature review, control allocation techniques have been applied to the design of ESC for yaw stabilization and the control of lateral acceleration. The control allocation approach enables both coordinated control of the suspensions and yaw stability control to be integrated into a single framework. The integration of yaw stability control and coordinated suspension control can be built into the control allocator. Redefining the virtual control signals and the vector of actuator controls to include both suspension and motor controls, we obtain a QP problem as with the standalone system, but of higher dimension. Though this presents a larger optimization problem, it is not nearly large enough to be intractable and can therefore be solved online using an active-set algorithm.

Once integrated, the combination of motor and suspension controls would constitute a robust rollover prevention system, through the combined control of lateral acceleration, yaw rate, and roll angle, the major factors in vehicle rollover. More generally, the integration of these systems would bring one step closer the realization of a complete vehicle dynamics control system. □

Bibliography

[1] Daimler AG. Active body control, http://techcenter.mercedes-benz.com/_en/abc/detail.html.

[2] A. Agrawal. *Performance Improvement of Automotive Suspension Systems using Inerters and an Adaptive Controller*. Master's thesis, University of Waterloo, Waterloo, ON, Canada, 2013.

[3] A. Agrawal and A. Khajepour. A new adaptive controller for performance improvement of automotive suspension systems with MR dampers. *SAE Intl. J. Passeng. Cars - Mech. Syst.*, 7(3), 2014.

[4] M. K. Binder and A. Khajepour. Optimal control allocation for coordinated suspension control. In *Proc. of the American Control Conference 2014*, Portland, OR, 2014.

[5] S. Boyd and L. Vandenberghe. *Convex Optimization*. Cambridge University Press, New York, 7th edition, 2009.

[6] Bose Corporation. Bose suspension system, http://www.bose.com/controller?url=/automotive/bose_suspension/index.jsp.

[7] H. J. Ferreau. *An Online Active Set Strategy for Fast Solution of Parametric Quadratic Programs with Applications to Predictive Engine Control*. Master's thesis, Universität Heidelberg, Heidelberg, Germany, 2006.

[8] G. J. Forkenbrock, W. Garrot, M. Heitz, and B. C. O'Harra. A comprehensive experimental examination of test maneuvers that may induce on-road, untripped, light vehicle rollover - phase IV of NHTSAs light vehicle rollover research program. Technical report, National Highway Traffic Safety Administration, 2002.

[9] O. Härkegård. Quadratic programming control allocation toolbox for MATLAB, http://research.harkegard.se/qcat/index.html.

[10] O. Härkegård. Efficient active set algorithms for solving constrained least squares problems in aircraft control allocation. In *Proc. of the Conf. on Decision and Control 2002*, Las Vegas, NV, 2002.

[11] O. Härkegård. *Backstepping and Control Allocation with Applications to Flight Control*. PhD thesis, Linköping University, Linköping, Sweden, 2003.

[12] O. Härkegård. Dynamic control allocation using quadratic programming. *Journal of Guidance, Control, and Dynamics*, 27(6):1028–1034, 2004.

[13] R. Jazar. *Vehicle Dynamics: Theory and Applications*. Springer, New York, 2008.

[14] T. A. Johansen and T. I. Fossen. Control allocation - a survey. *Automatica*, 49(5):1087–1103, 2013.

[15] W. D. Jones. Easy ride: Bose corp. uses speaker technology to give cars adaptive suspension. *IEEE Spectrum*, 42(5):12–14, 2005.

[16] H. K. Khalil. *Nonlinear Systems*. Prentice Hall, 3rd edition, 2002.

[17] C. Poussot-Vassal, C. Spelta, O. Sename, S. M. Savaresi, and L. Dugard. Survey and performance evaluation on some automotive semi-active suspension control methods: A comparative study on a single-corner model. *Annual Reviews in Control*, 36(1):148–160, 2012.

[18] B. Schofield. *Vehicle Dynamics Control for Rollover Prevention*. Licentiate thesis, Lund University, Lund, Sweden, December 2006.

[19] B. Schofield. *Model-Based Vehicle Dynamics Control for Active Safety*. PhD thesis, Lund University, Lund, Sweden, September 2008.

[20] B. Schofield and T. Hägglund. Vehicle dynamics control and control allocation for rollover prevention. In *Proc. of the 2006 Intl. Conf. on Control Applications*, pages 149–154, Munich, Germany, 2006.

[21] B. Schofield and T. Hägglund. Optimal control allocation in vehicle dynamics control for rollover mitigation. In *Proc. of the American Control Conference 2008*, pages 3231–3236, Seattle, WA, 2008.

[22] M. Strassberger and J. Guldner. BMW's dynamic drive: An active stabilizer bar system. *IEEE Transactions on Control Systems*, 24(4):28–29, 2004.

[23] J. Tjønnås and T. A. Johansen. Stabilization of automotive vehicles using active steering and adaptive brake control allocation. *IEEE Transactions on Control Systems*, 18:545–558, 2010.

[24] P. Tøndel and T. A. Johansen. Control allocation for yaw stabilization in automotive vehicles using multiparametric nonlinear programming. In *Proc. of the American Control Conference 2005*, Portland, OR, 2005.

[25] R. Wang and J. Wang. Fault-tolerant control for electric ground vehicles with independently actuated in-wheel motors. *ASME Journal of Dynamic Systems, Measurement, and Control*, 2012.

[26] W. Wong. *Theory of Ground Vehicles*. Wiley, New York, 3rd edition, 2001.